Journal of Volcanology and Geothermal Research 462 (2025) 108325

Contents lists available at ScienceDirect

Journal of Volcanology and Geothermal Research

journal homepage: www.journals.elsevier.com/journal-of-volcanology-and-geothermal-research

Volcanic gas changes prior to Stromboli's major explosions are statistically significant

Alessandro Aiuppa [a,*], Marcello Bitetto [a], Luciano Curcio [a], Dario Delle Donne [b], João Lages [a], Giovanni Lo Bue Trisciuzzi [a], Giancarlo Tamburello [c], Angelo Vitale [a], Flavio Cannavò [d], Mauro Coltelli [d], Diego Coppola [e], Lorenzo Innocenti [f], Laura Insinga [a], Giorgio Lacanna [f], Marco Laiolo [e], Francesco Massimetti [e,g], Marco Pistolesi [h], Eugenio Privitera [d], Maurizio Ripepe [f], Marija Voloschina [h], Giovanna Cilluffo [a,i]

[a] Dipartimento di Scienze della Terra e del Mare, DiSTeM, Università di Palermo, Italy
[b] Istituto Nazionale di Geofisica e Vulcanologia, Osservatorio Vesuviano, Italy
[c] Istituto Nazionale di Geofisica e Vulcanologia, Bologna, Italy
[d] Istituto Nazionale di Geofisica e Vulcanologia, Osservatorio Etneo, Catania, Italy
[e] Dipartimento di Scienze della Terra, Università di Torino, Italy
[f] Dipartimento di Scienze della Terra, Università di Firenze, Italy
[g] Instituto de Geofisica, Universidad Autonoma de Mexico, UNAM, Mexico
[h] Dipartimento di Scienze della Terra, Università di Pisa, Italy
[i] Consorzio Nazionale Interuniversitario per le Scienze del Mare- CONISMA-Roma, Italy

ARTICLE INFO

Keywords:
Volcanic gases
Statistical analysis
Eruption forecasting
Major explosions
Stromboli
CO_2
SO_2

ABSTRACT

The generally mild activity of mafic, open-vent volcanoes is punctuated by the periodic occurrence of sudden, larger-than-normal explosive eruptions. Examples of these sudden mafic explosive events are the so-called "major explosions" that occur (2 to 4 times a year on average) at Stromboli volcano in Italy. These relatively small explosions (Volcanic Explosivity Index, VEI < 1) occur without no obvious precursory change in surface activity, and therefore pose a threat to volcanologists/monitoring staff, and to the population in the most severe cases. Past work has found a link between periods of high CO_2/SO_2 ratios in the volcanic gas plume and the occurrence of such explosions, but this association has never been statistically verified. Here, we report on nearly continuous observations of volcanic gas plume CO_2 and SO_2 concentrations and ratios in a diluted plume, as well as SO_2 flux measurements, recorded in a four year (2020 to 2023) activity period of Stromboli volcano, during which 22 such major explosions took place. Using the Conditional Logit model and the Receiver Operating Characteristic (ROC) analysis, we establish a statistical association between the occurrence of major explosions and periods of reduced SO_2 concentrations (very significant) and fluxes, and high CO_2/SO_2 ratios (significant), in the volcanic plume. These findings are interpreted in light of a simplified conceptual model that explains major explosions as caused by gas bubble accumulation at a rheological discontinuity, resulting from deceleration of the shallow convecting magma that supplies the "regular" Strombolian activity. Using results of statistical analysis, we develop a volcanic gas-based Composite indicator that successfully forecasts (by a-posteriori analysis) 71 % of the events on timescales of week(s). However, we find that this Composite indicator is associated with a large (32 %) False Positive rate and hence low precision (20 %). The significant role of SO_2 concentrations in the model indicates that other factors, such as plume direction and inter-crater variations in gas composition, may need to be taken into account for improving the forecasting performance of the method. Thus, while our results emphasize the importance of gas plume observations in volcano monitoring, they also highlight their current limitations as eruption forecasting tools.

* Corresponding author.
E-mail address: alessandro.aiuppa@unipa.it (A. Aiuppa).

https://doi.org/10.1016/j.jvolgeores.2025.108325
Received 28 November 2024; Received in revised form 24 February 2025; Accepted 24 March 2025
Available online 25 March 2025

1. Introduction

Active, potentially harmful volcanoes worldwide are monitored by increasingly sophisticated monitoring networks (Sparks et al., 2012; Acocella et al., 2024), with the goal of detecting changes in patterns and trends of monitored parameters in the run-up to eruption (Sparks and Cashman, 2017; Poland and Anderson, 2020). In addition to seismicity (Matoza and Roman, 2022), ground deformation (Biggs and Pritchard, 2017) and thermal emissions (Reath et al., 2019), volcanic gas geochemistry has long been recognised (e.g., Menyailov, 1975) as a potentially very useful volcano monitoring tool (Edmonds, 2021; Kern et al., 2022). Magmatic volatiles have finite solubilities in magmas, causing them to partition into a separate volatile phase at upper mantle to crustal conditions (Papale et al., 2022). This magmatic degassing process (Oppenheimer et al., 2014) is a critical driver of magma evolution during storage and pre-eruptive ascent, and plays a key control on if, and with which modalities and rates, magma will ultimately erupt (Edmonds and Wallace, 2017). From a volcano monitoring perspective, the intrinsically mobile nature of gas bubbles implies that they can separate and escape from deeply stored magma (Edmonds et al., 2022) to be eventually emitted at the surface well before magma.

There is vast, documented evidence in the geological literature on the use of volcanic gas chemistry as eruption precursor (Edmonds, 2021). Reported observations are the most diverse in terms of methodology used, targeted emission type (fumaroles, plumes, soil diffuse emissions, groundwaters), and measurement temporal resolution; these range from multi-species, long-term monitoring of fumarole compositions, through periodic (monthly to yearly) direct sampling surveys (e.g., Vaselli et al., 2010) to single species (e.g., SO_2 flux) near-real time (temporal resolution of seconds to minutes) observations with instrumental networks (e.g., Delle Donne et al., 2017; Arellano et al., 2021). An especially useful advance has come with the advent of compact, multi-sensor gas sensing units (e.g., Multi-GAS) that can be used for near real-time temporal monitoring of the CO_2/SO_2 ratio in volcanic gas plumes (e.g., Aiuppa et al., 2007, 2010, 2021; de Moor et al., 2016a,de Moor et al., 2016b, de Moor et al., 2019).

Notwithstanding their significant potential, the use of volcanic gas observations as truly exploitable eruption forecasting tools is challenged by a lack of quantitative data analysis testing the statistical robustness of any identified gas "precursor" (although notable exceptions exist; Kunrat et al., 2022). This partly reflects the relatively novel and immature technology in volcanic gas science, which requires frequent field maintenance from expert operators and has hitherto hampered wider (global) deployment of gas sensing networks. As such, complete (temporally continuous) long-term volcanic gas datasets are limited to only a few, well-instrumented volcanoes. This, in conjunction with the relatively infrequent volcanic events occurring at any given volcano, has led to monitoring gas data being insufficient (in number, continuity, and quality) to systematically test patterns indicative of a certain volcanic behaviour. In many cases, the reported "precursory" gas variations refer to only one specific eruptive event (e.g., Aiuppa et al., 2017; Aiuppa et al., 2018), leaving the question on their systematicity and repeatability unanswered.

Stromboli volcano in Sicily (Southern Italy) hosts a well-instrumented volcanic gas monitoring network (Allard et al., 2008; Aiuppa et al., 2009, 2010, 2021; Burton et al., 2009; Inguaggiato et al., 2013, 2017; Delle Donne et al., 2017, 2022; Federico et al., 2023; Lo Bue Trisciuzzi et al., 2024) and, owing to its relatively steady and well-understood eruptive behaviour (Rosi et al., 2013; Pioli et al., 2014), is an ideal test site to quantitatively explore the link between volcanic gas variations and volcano behaviour. Here, we focus on an intermediate class of explosive events referred as "Major Explosions" that, in view of their eruption dynamics (Bertagnini et al., 1999; Andronico and Pistolesi, 2010) and relatively high occurrence rate (Bevilacqua et al., 2020), represent one of the most hazardous volcanic phenomena at this volcano (Rosi et al., 2013). It has been previously shown (Aiuppa et al., 2011) that major explosions are often anticipated – by days to weeks – by remarkable increases in the volcanic gas plume CO_2/SO_2 ratio; these have been explained as being due to precursory leakage of CO_2-rich gas bubbles from an accumulating foam on top of a deeply stored (> 3 km depth) mafic magma (whose later, rapid ascent then triggers the explosion itself) (Aiuppa et al., 2010; Aiuppa et al., 2011; Aiuppa et al., 2021).

Here, we analyse the statistical association between the temporal variations in plume chemistry/flux at Stromboli and the occurrence of major explosions from January 2020 to December 2023. Our aim is to quantitatively test the potential utility of volcanic gas plume geochemistry as an exploitable eruption forecasting tool.

2. Stromboli's major explosions

Stromboli's major explosions are transient, impulsive (total duration of tens of seconds) explosions that produce discrete (unsustained) eruptive columns ~200 m in height on average (Fig. 1). These violent blasts typically erupt moderate volumes (10^2 to $\leq 10^4$ m^3) of mostly coarse, vesicular pyroclastic fragments and ballistics that cover the crater terrace and the volcano's slope without leaving a continuous blanket of tephra deposits (Bertagnini et al., 1999; Andronico and Pistolesi, 2010; Rosi et al., 2013; Pioli et al., 2014). Major explosions thus share similar eruption dynamics with, but have larger dispersal areas and higher erupting volumes than, the regular Strombolian explosions (~10 m^3) that exemplify Stromboli's ordinary activity (Ripepe et al., 2008). Major explosions occur at an average rate of ~1–4 events per year (~140 events catalogued in the 1879–2020 period; Bevilacqua et al., 2020) and interrupt suddenly, and with no visible precursory change in surface activity, the regular Strombolian open-vent activity. In the very short-term (< 300 s before), each major explosion is typically anticipated by mild ground uplift (<1 μrad), interpreted as caused by pressure build-up in the upper conduit system due to rapid expansion of gas and/or volatile-rich magma into the shallow stored conduit magma (Ripepe et al., 2021). Whereas magma fragmentation is unquestionably a shallow process, there is debate on whether overpressure develops in the shallow conduit itself (i.e., in response to formation of a viscous plug, and hence permeability drop; Falsaperla and Spampinato, 2003; Calvari et al., 2012), or if instead it is triggered by the arrival of more deeply sourced gas/magma. The latter hypothesis is corroborated by the frequent eruption of highly vesicular (pumiceous) Low Porphiricity (LP) magma fragments during most major explosions (Andronico and Pistolesi, 2010; Landi et al., 2008; La Felice and Landi, 2011; Pioli et al., 2014; Voloschina et al., 2023; Insinga et al., 2024). This LP magma component is instead always ejected during paroxysmal eruptions (the most intense manifestations of Stromboli volcano) and, according to petrological (Métrich et al., 2001, 2010, 2021; Voloschina et al., 2023) and experimental (Pichavant et al., 2009, 2022) evidence, cannot derive from previously shallow stored magma, but rather requires rapid ascent from a > 3 km deep magma storage zone. The emission of CO_2-rich gas prior to major explosions (Aiuppa et al., 2011, 2021; Voloschina et al., 2023) is also an indication of a deeply operating process in the run-up to the explosion. These precursory gas changes are the object of this study.

In the four year temporal window covered by this study (2020 to 2023), there were a total of 22 major explosions, with an occurrence rate (estimated on a 3-month basis) of 0 to 4 events (Fig. 2a). As previously found (Bevilacqua et al., 2020), these events occur in clusters, in which several events repeat in relatively narrow intervals (of days to a few months). In our study interval, we identify three main clusters (labelled as *I*, *II* and *III* in Fig. 2a) in July–December 2020, July–October 2021, and May 2022–April 2023, interspersed within periods with no (or less frequent) events. We include two impulsive explosive events (orange stars; on October 9 and December 4, 2022) in our statistics during which no vertically rising eruptive clouds were observed (as normally occurs during major explosions), but rather the rapid formation of turbulent, hot pyroclastic density currents (PDC) from the active vents (Fig. 1,

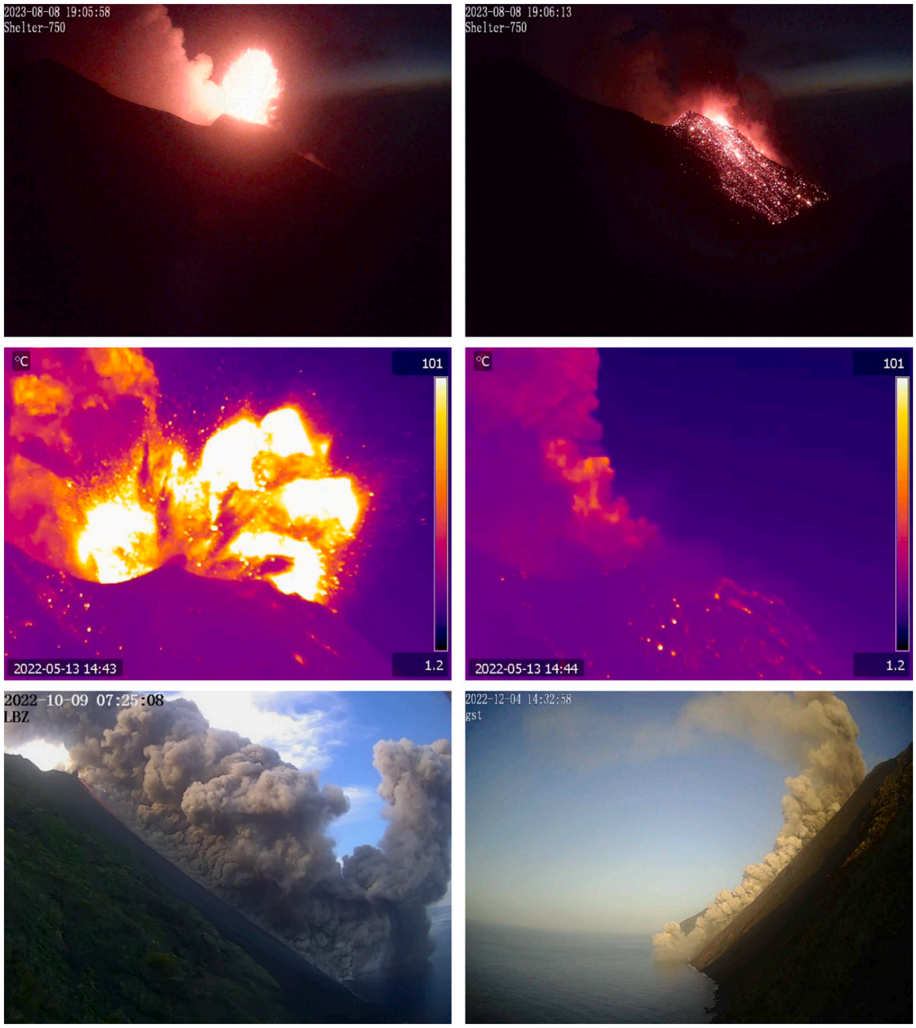

Fig. 1. Images of selected major explosions, as recorded by the LGS monitoring cameras (http://lgs.geo.unifi.it/). Top images, the 8 August 2023 major explosion, showing eruption onset (left) and the fallout dispersal area (right). Central images, the 13 May 2022 major explosion, showing the eruption onset (left) and the fallout dispersal area (right); Bottom images, pyroclastic density currents in the Sciara del Fuoco, formed during the October 2022 and 4 December 2022 collapse events.

bottom panels). These PDCs, rapidly emplaced along the Sciara del Fuoco scar, also led to a sequence of small tsunamis entering the sea, as indicated by monitoring reports of the Laboratorio Geofisica Sperimentale (LGS, Università di Firenze) (see also Global Volcanism Program, 2023). Our analysis is hence based on 24 non-regular explosive events in total.

3. Methods

3.1. Volcanic gas dataset

Statistical analysis is applied to a volcanic gas dataset (Figs. 2b-e and 3) acquired by the geochemical monitoring network run by DiSTeM-Università di Palermo, between January 2020 and December 2023.

The SO_2 flux time-series (Fig. 2b) is obtained by processing sets of images acquired by a permanent, fully automated UV Camera system. Functionalities of the UV Camera, including data acquisition and processing routines, have been described elsewhere (Delle Donne et al., 2017, 2022; Lo Bue Trisciuzzi et al., 2024). Results, listed in Supplementary Table S1 and illustrated in Fig. 2b, are expressed in the form of daily averaged SO_2 fluxes (metric tonnes per day, t/d), obtained by averaging all successful flux quantifications obtained (at 0.5 Hz rate) during 6 h-long daily temporal windows (acquisition limited to best sunlight illumination conditions).

Figs. 2c-e are time-series of plume SO_2 and CO_2 concentrations (in ppmv), and of their relative proportions in the plume (the molar CO_2/SO_2 ratio), obtained by processing data streamed by two fully automated Multi-GAS units, located in the summit crater area (~500 m distance from the crater terrace). The Multi-GAS units (see Aiuppa et al., 2021 for detailed descriptions) are configured to capture (at 1 Hz rate) the output signals from a set of pre-calibrated, gas-specific sensors, mounted in series, and exposed to the target gas plume. Acquisitions are automatically activated (by a datalogger) at regular intervals (typically every 4 h), and their duration is modulable (from ~300 to 1800 s), depending on the SO_2 concentration levels encountered to save power (the unit is programmed to halt acquisitions below a pre-set concentration threshold). The sensors' output signals (counts, or mV) are automatically converted into gas concentrations (ppmv) using lab-determined calibration functions (stored in the datalogger). These concentration time-series are then processed in near-real time by a R-based script that sequentially scans the dataset using a 60 s-long moving window, searching for (and identifying) intervals with (i) high temporal coherence (Pearson correlation coefficient $\geq$ 0.9) between CO_2 and SO_2 concentrations time series, and (ii) SO_2 concentrations at/above a 1 ppm threshold. We note that more conservative (higher) SO_2 concentration thresholds have been used in previous work (e.g., Aiuppa et al., 2009). For each 60 s temporal window in which both conditions above are met, the algorithm saves the maximum SO_2 concentration (shown in Fig. 2c),

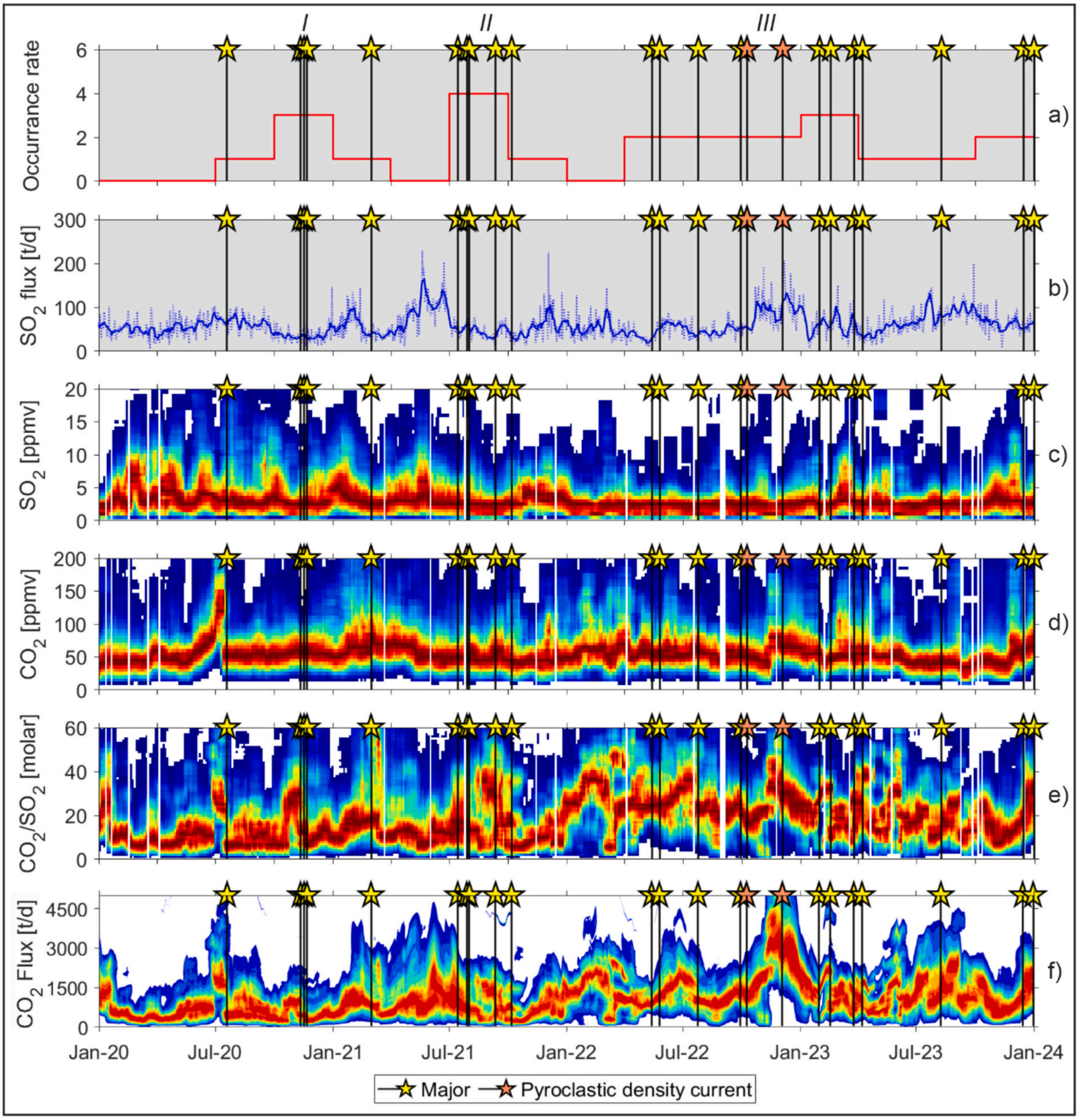

Fig. 2. Four years (2020–2023) of gas observations at Stromboli. (a) Rate of occurrence (number of events/3 months) of major explosions. Yellow and orange stars identify major explosions and collapse/pyroclastic density currents, respectively. Three main clusters are identified (labelled *I*, *II* and *III*); (b) Daily averaged SO_2 fluxes (t/d) measured by Stromboli's permanent UV camera (the solid line is 30 day moving average); (c) to (f), temporal plots of (normalized) frequency distribution diagrams of (c) SO_2 and (d) CO_2 concentrations in the plume, CO_2/SO_2 (molar) ratios (e) and CO_2 fluxes (f). Dark red tones show information on the temporal fluctuations of the dominant concentration/ratio levels, whilst orange to blue tones indicate increasingly less represented frequency bins. (For interpretation of the references to colour in this figure legend, the reader is referred to the web version of this article.)

the range (maximum – minimum) ΔSO_2 and ΔCO_2 concentration levels (the latter shown in Fig. 2d), and calculates the corresponding CO_2/SO_2 molar ratio (Fig. 2e) (Aiuppa et al., 2021). Use of the ΔCO_2 concentration helps to resolve the volcanic concentration signal (as expressed by the maximum) above the atmospheric background (as approximated by the minimum; note the atmospheric background is negligible for SO_2). The ratio is obtained from the slope of the best-fit linear regression function calculated from the ΔSO_2 and ΔCO_2 concentration time series within the processing window (Aiuppa et al., 2021). Circa 155,000 triplets (maximum SO_2 and ΔCO_2 concentrations, and CO_2/SO_2 ratios) of data were obtained during 2020–2023, all listed in Supplementary Table S2 and in Figure S1. Supplementary Tables S3, S4 and S5 list the statistical parameters of SO_2 and CO_2 concentrations and CO_2/SO_2 ratios, all calculated on a 3-day basis (the statistical parameters are assigned to the first of the 3 measurement days). We utilize the graphic representation from Aiuppa et al. (2021) solely for illustrative purposes, rather than statistical analysis, to highlight temporal changes in plume chemistry. In these plots, data (Supplementary Table S2) are presented as chronograms of normalized frequency distribution diagrams (Figs. 2c-e). To this aim, sets of individual frequency distribution plots are initially calculated from all concentration/ratio results obtained within each 3-day interval. Next, a centered smoothing function is applied to sets of 5 adjacent frequency distribution plots (covering 15 days in total) to filter out short-term (hourly to daily) fluctuations and emphasize longer term (multi-day to weekly/monthly) trends. In the resulting plots (Figs. 2c-e and Fig. 3), warmer tones (dark red) correspond to the

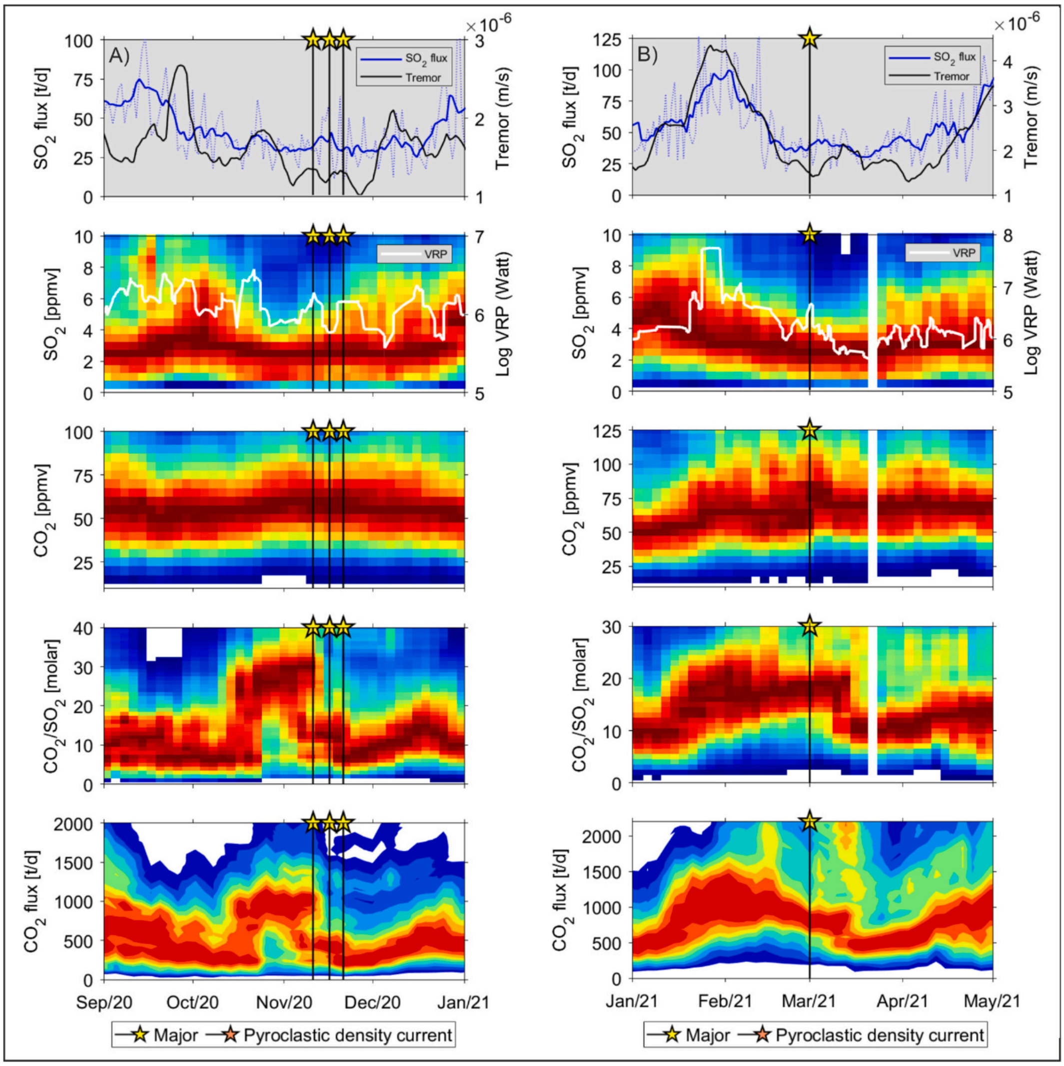

Fig. 3. A zoom of the compositional evolution of Stromboli's plume (Fig. 2) in two selected intervals. The temporal record of volcanic tremor amplitude and the Volcanic Radiative Power (VRP, Watt), derived from satellite thermal observations, are also shown for comparison.

median of the frequency distribution, while cooler colours (yellow to green to blue tones) correspond to progressively less represented frequency bins. The plots therefore convey information on temporal fluctuations of: (i) the most-represented concentration levels/ratios, and (ii) on the spread around them.

Finally, the volcanic CO_2 flux (Fig. 2f and Supplementary Table S1) is obtained by combining the CO_2/SO_2 ratio record of Fig. 2e with the daily-averaged SO_2 flux (Fig. 2b).

We note that the fraction of data gaps in the Multi-GAS time series is $<$5 % of the total observations. According to theory (Bennett, 2001), this low data gap fraction has marginal impact on the statistical analysis discussed below.

3.2. Statistical analysis

We use a Conditional Logit model (Logan, 1983) to investigate the statistical link between the occurrence of major explosions at Stromboli and the temporal changes in gas composition and flux. More specifically, independent models are explored that separately analyse the association between major explosions and: 1) the SO_2 flux (daily averages; Supplementary Table S1); 2) the maximum plume SO_2 concentration, 3) the plume ΔCO_2 concentration, 4) the plume CO_2/SO_2 ratio, and 5) the CO_2 flux. For SO_2 and ΔCO_2 concentrations, and for the plume CO_2/SO_2 ratio, the non-averaged data reported in Supplementary Table S2 are used.

The Conditional Logit model (Logan, 1983) is commonly used in the context of time-series analysis to model categorical outcomes over time. If applied to a dataset consisting of a temporal sequence of repeated observations (as is the case in volcano monitoring), the model can be used to infer how/if different levels of a certain parameter influence the likelihood of a certain event. Lagged variables, in the context of statistical analysis or time-series modeling, refer to variables that are delayed in time. In the Conditional Logit model, lagged variables are typically utilized to capture the effect of past exposure on a given event. In our specific case, our analysis aims to estimate if the probability of having a major explosion at a given time t increases when/if a specific geochemical pattern (e.g., high/low levels of gas concentration/ratio/flux) is observed at time *t-Lag* (where Lag is the lag time). In our case, a lagged variable corresponds to the daily average of the given parameter at *t-Lag*. The lagged effects are evaluated to up to 15 days (Fig. 4a) and our models take the following form:

$$logit(P(eventattimet)) = \beta_0 + \beta_1 Lag_1 + \beta_2 Lag_2 + \ldots + \beta_{15} Lag_{15} \quad (1)$$

where $P(eventattimet)$ is the probability of having a major explosion at time t, logit is the natural logarithm of the odds of the event occurring, and the β_i are the coefficients corresponding to each lagged variable, representing the impact of that variable on the log odds of the event occurring. To estimate β_i, we solve for the values that maximize the log-

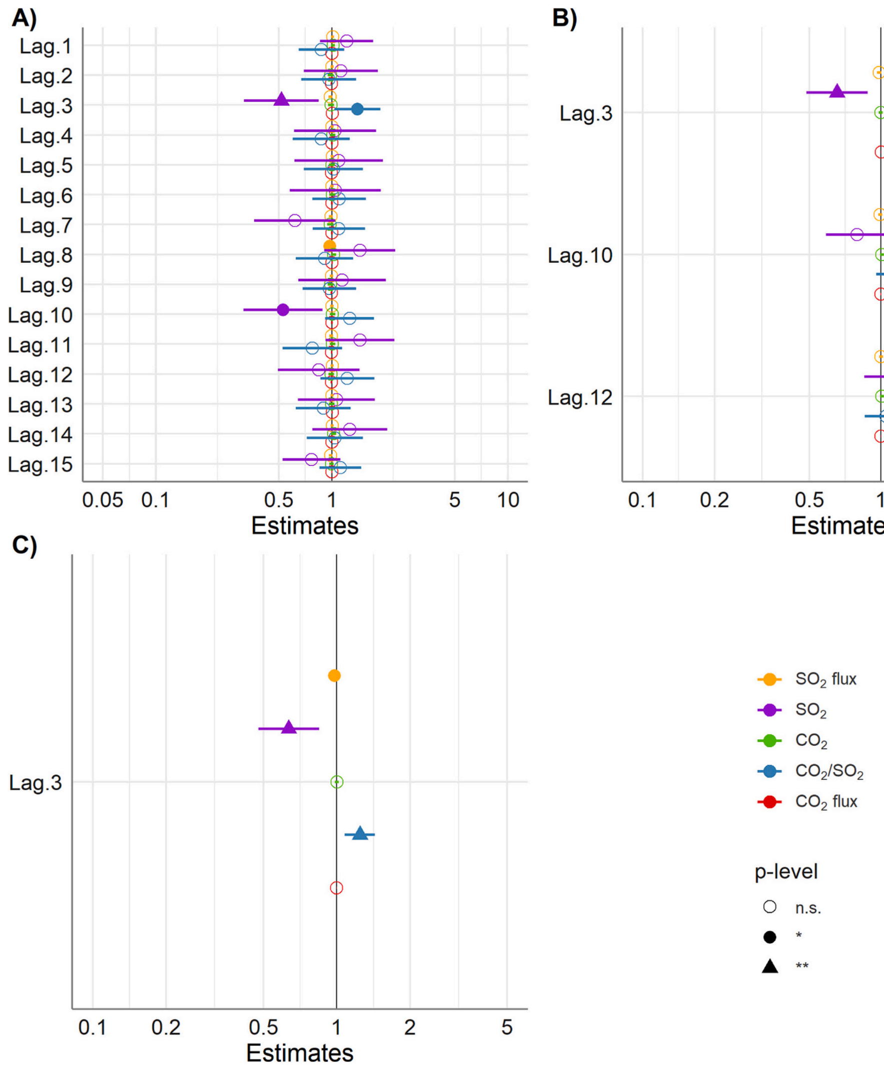

Fig. 4. OR and 95 % confidence intervals of the four full conditional logistic regression models. p-levels: Open symbols, n.s., not significant. Filled circles, statistically significant (circles and tringles indicate increasing levels of significance, denoted by one or two asterisks).

likelihood function through an iterative optimization algorithm. To obtain the odds of the event occurring, which indicate how the odds of the event occurring change for a one-unit increase in each lagged variable, holding all other lagged variables constant, we use the following formula:

$$OR_i = e^{\beta_i} \tag{2}$$

where OR_i is the odds ratio associated with the lagged variable Lag_i (Fig. 4).

In a separate analysis, the odds ratio (OR) and 95 % confidence intervals are calculated using as explanatory variables the right-aligned moving averages (7, 15 and 30 days) of the five parameters analysed (see Fig. 5), instead of using the lagged variables. Use of the moving average allows testing if the temporal persistence (over timescales of 7 to 30 days) of a specific geochemical pattern impacts the probability of a major explosion happening at time *t*. This analysis is hence complementary to that obtained using the lagged variables, that are based instead on observations made at a specific *t-lag* time. Note that, in both types of analysis, each major explosion is treated as a separate case, even if part of a cluster of closely spaced explosions (Fig. 2a).

Statistical significance is set at *p*-value <0.05 (α), where the p-value is a measure of the strength of evidence against the null hypothesis ($\beta_i = 0$ *or* $OR_i = 1$ in our case). In other words, the p-value tells us if the association between the considered explanatory variable(s) and the

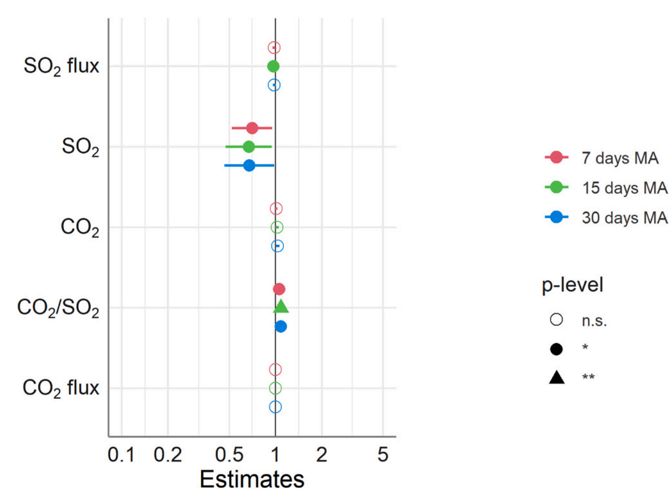

Fig. 5. OR and 95 % confidence intervals for 7, 15 and 30 days moving averages of the four parameters analysed. p-levels: Open symbols, n.s., not significant; filled circles, statistically significant.

event is statistically significant. The α level is the predetermined threshold used to assess the statistical significance of the p-value and represents a Type I error, i.e., the probability of rejecting the null hypothesis when the null hypothesis is true.

We also perform a ROC (Receiver Operating Characteristic) analysis (Fig. 6) with the aim of testing the ability of the monitored variables (SO_2 flux, SO_2, CO_2 and CO_2/SO_2) to "predict" the likelihood of a major explosion, and hence select their optimal cutoff values. These correspond to the values of the plume SO_2 flux, SO_2, CO_2 and CO_2/SO_2 closest to the perfect ROC curve (having both sensitivity and specificity equal to 1). The ROC analysis is conducted on both the lagged variables (Lag3, Lag5 and Lag7; Fig. 6a-d) and on the moving averages of each parameter (moving averages at 7, 15 and 30 days; Fig. 6e-h). A ROC curve (Fig. 6) is a graphical tool that illustrates the performance of a binary classifier model, and it is built by plotting the True Positive rate (TPR, or sensitivity) against the False Positive rate (FPR, or 1 - specificity) at varying threshold values. In our application, TPR (sensitivity) and FPR (or 1 – specificity) are defined as the proportion of actual major explosions correctly identified by the model using the optimal cut-off, and the proportion of actual non-major events correctly identified by the model, respectively. Performance of the binary classification model across all possible threshold values is estimated using the area under the curve (AUC) (significance expressed by AUC > 0.5; tested using the method described by DeLong et al., 1988) (Supplementary Table S6 and S7).

Ultimately, four reduced models based on the significant lagged variables are obtained and the relative risks (RR; Fig. 7a-d) are derived as follows:

$$RelativeRisk = \frac{P_{event=1}}{P_{event=0}} \tag{3}$$

Using a similar formula, the RR for the statistically significant (Fig. 5) moving averages are also obtained (Fig. 7e-h).

We finally implement a Composite indicator (Fig. 8) to combine the relative risk of the significant models, using an Additive Value Model (AVM) (Cilluffo et al., 2024). The AVM is a linear approach that quantifies the combined effect of multiple factors. Steps in the analysis include: (i) identifying the relevant dimensions, (ii) assigning their weights, (iii) linearly combining the weighted parameters, and (iv) interpretating the results. The resulting value provides a concise representation for communication and evaluation. In our study, we identify the 15-day moving average SO_2 relative risk (orange in Fig. 7f) and the 15-day moving average CO_2/SO_2 ratio relative risk (orange in Fig. 7h) as key attributes for our composite indicator, and the weights are optimised to maximize accuracy. The final Composite indicator assumes values between 0 and 1 (Fig. 8). High values indicate increased eruption probabilities, while low values identify background activity with low eruption probability.

All the statistical analyses were performed with the R version 4.0.2 (R Foundation for Statistical Computing, Vienna, Austria). Statistical significance is set at $p < 0.05$.

3.3. Volcanic tremor and volcanic radiative power (VRP)

To better characterise Stromboli's activity in the run-up to a major explosion, we complement our volcanic gas results with the temporal record of volcanic tremor and volcanic radiative power (VRP). Volcanic tremor, the most typical seismic parameter recorded on active volcanoes, is generally related with the upward migration of magma and gases in the plumbing system and hence provides useful information on volcanic activity evolution (McNutt, 2002; McNutt and Nishimura, 2008). Links between degassing and tremor have been investigated in different volcanic systems (Williams-Jones et al., 2001; Edmonds et al., 2003; Patanè et al., 2013; Zuccarello et al., 2013; Delle Donne et al., 2022), and increases in seismic tremor amplitude are typically observed prior to and during eruption (e.g., Brandsdóttir and Einarsson, 1992; Fischer et al., 1994; Bonaccorso et al., 2011; Nadeau et al., 2015; Valade et al., 2016; Ripepe et al., 2009; Aiuppa et al., 2023). Tremor at Stromboli is interpreted to be caused by the self-induced resonance oscillations of a bubble cloud (Chouet et al., 1997) in the shallow conduit (<200 m) or by the repeating pressure drop of self-coalesced gas bubbles bursting at the surface of the magmatic column (Gordeev, 1993; Ripepe and Gordeev, 1999). The strong correlation of tremor amplitude with infrasonic pressure energy released in the atmosphere implies a causal link with degassing processes in the shallow portion of the magmatic column (Ripepe et al., 1996). Several studies (e.g., Delle Donne et al., 2022; Aiuppa et al., 2023, Lo Bue Trisciuzzi et al., 2024) have found experimental evidence for the correlation between volcanic tremor and degassing processes, and the temporal increases of both parameters are typically associated with phases of escalating magmatic activity (Ripepe et al., 2009). We use the daily average of RMS (Root Mean Square) tremor amplitude, calculated on 1-min-long time window of seismic signal filtered in band 0.9–10 Hz (Figs. 3, 9). This frequency band includes the main spectral content of volcanic tremor energy at Stromboli (Chouet et al., 1997). Data streamed from the LGS ROC station is used.

The heat flux produced by volcanic activity is generally measured by means of the Volcanic Radiative Power (VRP), a composite measure of the area and temperature of the observed volcanic source (Coppola et al., 2023). Here we use the data from the MIROVA system (Middle Infrared Observations of Volcanic Activity) which ingests infrared data acquired by the Moderate Resolution Imaging Spectroradiometer (MODIS) and Visible Infrared Imaging Radiometer Suite (VIIRS) sensors to provide near-real time estimates of the VRP (Campus et al., 2022; Coppola et al., 2023). Previous studies at Stromboli have shown that the ordinary, mild-explosive activity is typically associated with VRP in the 1–30 MW range, with periodic fluctuations strictly related to variations in the level of the convective magma column that feeds the craters (Coppola et al., 2014, 2016; Laiolo et al., 2022; Massimetti et al., 2024). Higher VRP values (e.g. close to 100 MW) are typically associated with sustained spattering activity that often precedes short-lived lava overflows or longer effusive eruptions (Laiolo et al., 2022).

4. Results

The daily averaged SO_2 fluxes fluctuate widely during 2020–2023, ranging from 6 to 230 tons/day (mean, 60 ± 30 t/d; Fig. 2b). The maximum in plume SO_2 concentrations also vary widely, from 1 ppmv (the selected concentration threshold) to 38.6 ppmv (Supplementary Fig. S1). The median SO_2 concentrations (3-day intervals; dark red tones in Fig. 2c) fluctuate at around 1.9 to 6.8 ppmv level (see Supplementary Table S3). SO_2 concentrations >10 ppmv are hence statistically less frequent (Fig. 2c) at the Multi-GAS measurement points. The ΔCO_2 concentrations (Fig. 2d) vary from <10 ppmv to >200 ppmv (see Supplementary Table S4), with the median level (dark red tones in Fig. 2d) typically oscillating at ~50 ppmv (range, 35 to 129 ppmv; see Supplementary Fig. S1). The largest ΔCO_2 concentrations are observed in the weeks prior to the July 19, 2020 major explosion, the largest of this class of events (in the 2020–2023 interval) from instrumental (Ripepe et al., 2021) and physical volcanology (Voloschina et al., 2023) viewpoints. Our extensive dataset confines the mean and median plume CO_2/SO_2 (molar) ratios at 20.9 and 17.7, respectively. The ratio range is extremely wide (1.2 to 809; Supplementary Table S2), and the 3 day interval medians (dark red tones in Fig. 2e) range from ~7 to ~38 (Supplementary Table S5). The median CO_2/SO_2 ratio levels are characteristically higher in 2022 to early 2023 (Fig. 2e), in conjunction with a main cluster of major explosions (Fig. 2a).

Qualitative, visual inspection of Fig. 2 highlights non-uniform, case-specific plume composition behaviour prior to each of the 24 studied explosive events. We yet identify some commonalities, such as the elevated CO_2/SO_2 ratio observed in the days to weeks preceding several major explosions (Fig. 2e), as previously found (Aiuppa et al., 2011; Voloschina et al., 2023). To illustrate this aspect more clearly, we selected two cases (Fig. 3a-b and Supplementary Fig. S2) where the gas

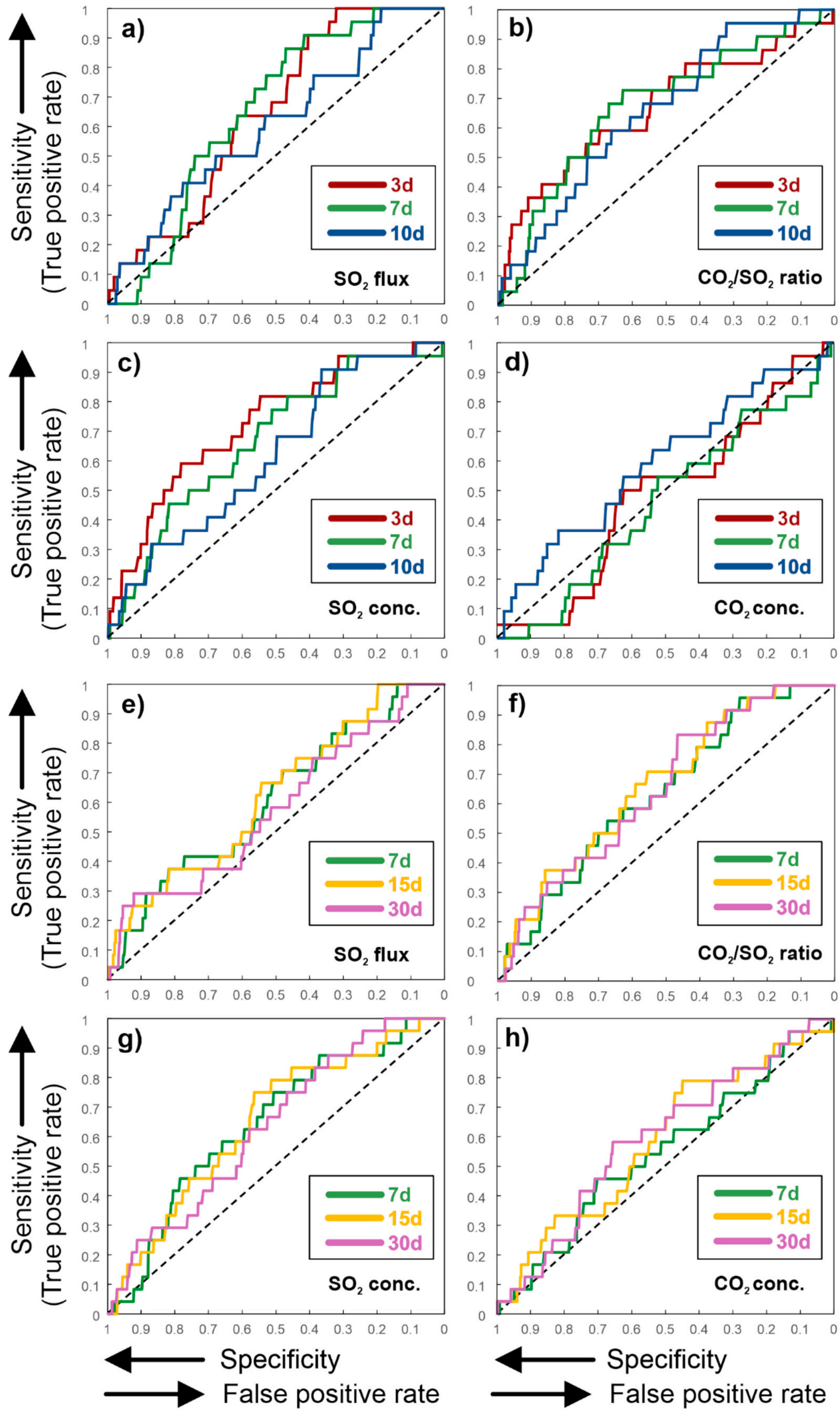

Fig. 6. Receiver Operating Characteristic (ROC) curves illustrating the ability of the four monitored volcanic gas parameters to predict the occurrence of major explosions. Plots a) to d) are based on the lagged variables, while e) to h) are based on 7, 15, 30 days moving averages.

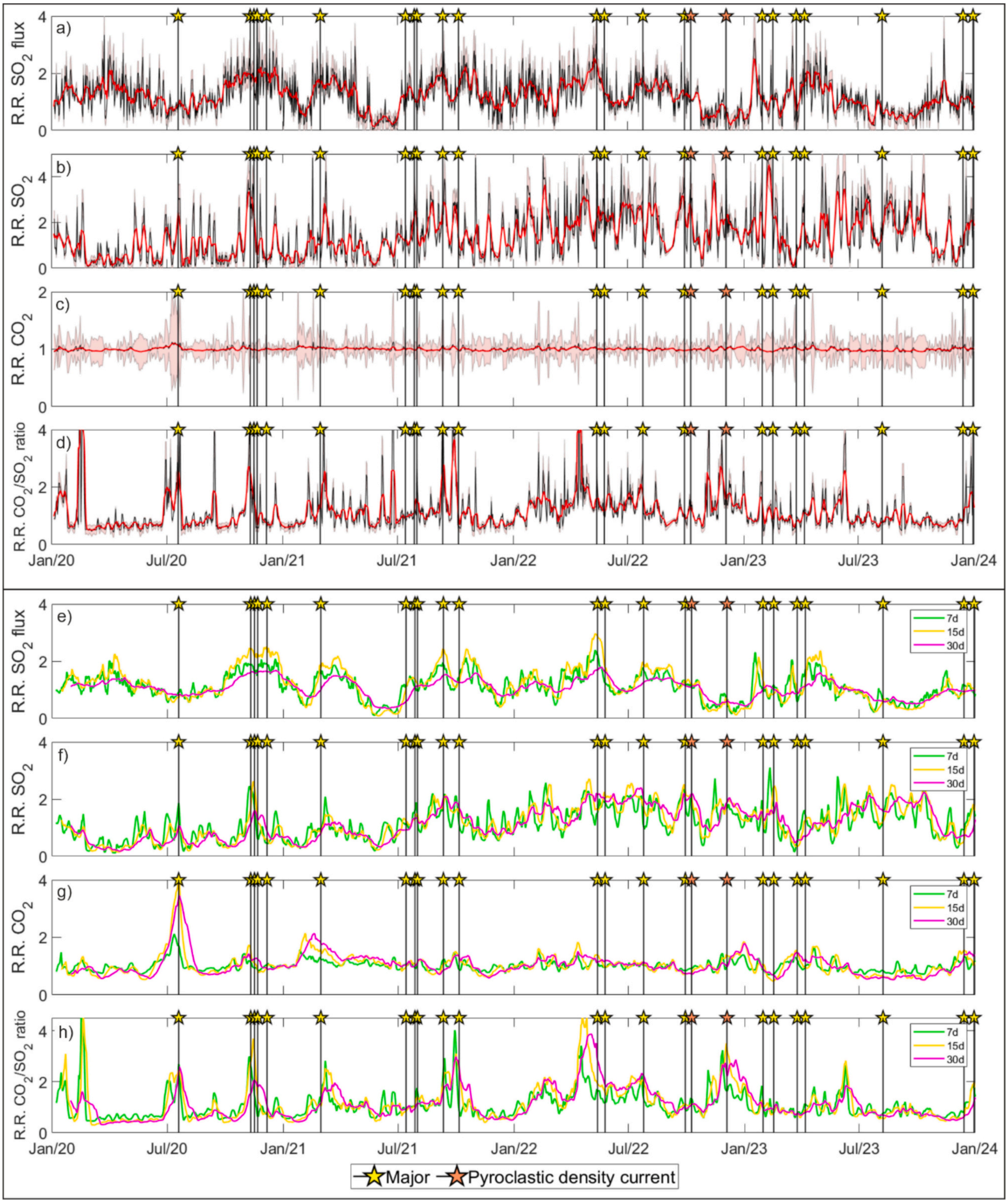

Fig. 7. Time-series of the Relative Risks (RR) (see. Eq. 3) for the four distinct Lagged (3 days) variables (a to d) and for the 7, 15, 30 days moving averages (e to h).

plume compositional changes prior to/after an explosive event are more evident. An especially well-behaved gas plume evolution is observed corresponding to three major explosions in November 2020 (Fig. 3a). The plume CO_2/SO_2 ratio visibly increases starting from ~3 weeks before the first explosion, from ~10 (and certainly <<20) to ≥30. This CO_2/SO_2 ratio increase is also concurrent with a phase of decreased SO_2 fluxes and plume SO_2 concentrations, and of slightly (but appreciably) increasing plume CO_2 concentrations and fluxes (Fig. 3a). Hence, the three explosions all occurred during a phase of reduced SO_2 release relative to CO_2. Importantly, this behaviour is not unique to the November 2020 explosions. For example, remarkably similar plume evolutions are observed prior to explosions in early 2021 (Fig. 3b) and in mid-to-late 2021 (Supplementary Fig. 2a). More complex and ambiguous compositional trends are observed in other temporal intervals

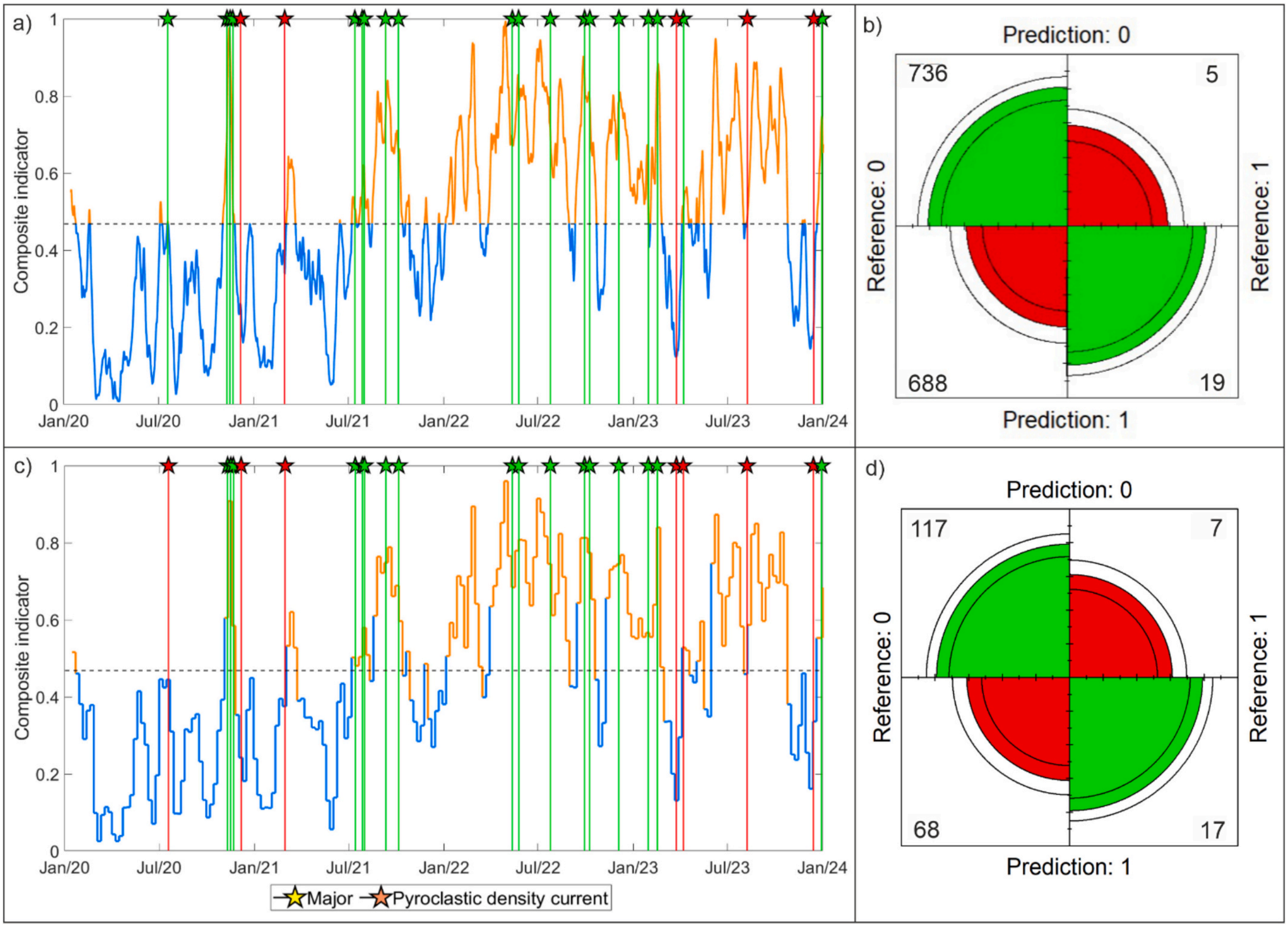

Fig. 8. (a) Time-series of the Composite indicator, calculated on a daily basis. The Composite indicator is obtained by linear combination of the 15 day moving average SO_2 Relative Risk (light orange in Fig. 7f) and of the 15 day moving average CO_2/SO_2 ratio Relative Risk (light orange in Fig. 7h). The blue/red colour tones correspond to values below/above the optimal threshold (0.468). The 24 explosive events are indicated by stars; green stars indicate explosions occurring on days with above threshold composite indicator (True Positives, 19 events), while red stars indicate explosions occurring on days with below threshold composite indicator (False Negatives, 5 events); (b) Confusion matrix computed from the daily values of the Composite indicator (panel a); (c) Weekly averaged time-series of the Composite indicator. Blue/red line as in panel a. Green and red stars are explosions identified as True Positives (17) and False Negatives (7), respectively, as based on the confusion matrix of panel (d). This confusion matrix is based on the temporal persistence of the Composite Indicator. True positives are explosions preceded by 7 consecutive days with above threshold Composite indicator, while false negatives are explosions that are not preceded by 7 consecutive days with above threshold Composite indicator. (For interpretation of the references to colour in this figure legend, the reader is referred to the web version of this article.)

(Supplementary Fig. 2b-d). In the October 2022 to April 2023 period (Supplementary Fig. 2c), increasing CO_2/SO_2 ratios are still observed weeks prior to all events recorded; however, while SO_2 fluxes and SO_2 concentrations drop down in correspondence to the two winter 2023 explosions, they do not prior to the December 4, 2022 event. The January–July 2022 (Supplementary Fig. 2b) and May–October 2023 (Supplementary Fig. 2d) events are examples of major explosions which are not preceded by any obvious precursory CO_2/SO_2 ratio change. Rather, in both periods we identify phases (e.g., January to March 2022) in which the CO_2/SO_2 ratio is sustainedly high, and yet no major explosion is observed.

Results of the application of the Conditional Logit model to the volcanic gas compositional time-series are illustrated in Figs. 4 and 5. We find a statistically significant association between the occurrence of major explosions and volcanic gas composition (SO_2 concentration and CO_2/SO_2 ratio) at Lag 3 levels (Fig. 4a, b). Since only Lag 3 shows significant results, we estimate five reduced models (Fig. 4c) including only Lag 3 of all explanatory variables (SO_2 flux, SO_2, CO_2 and CO_2/SO_2 ratio, CO_2 flux). Of the reduced models (Fig. 4c), a unit decrease in SO_2 concentration is significantly associated with an increased probability of having a major explosion at Lag 3 (OR = 0.635, 95 % CI: 0.476–0.848, p = 0.002). Likewise, a unit decrease in the SO_2 flux is significantly associated with an increased probability of having a major eruption. By contrast, a 5 unit increase in the CO_2/SO_2 ratio is significantly associated with an increased probability of having a major explosion over the same (Lag 3) temporal window (OR = 1.243, 95 % CI: 1.078–1.434, p = 0.003) (Fig. 4). CO_2 concentrations and CO_2 flux do not exhibit any statistically significant relationship with the occurrence of major explosions.

The same models applied to moving averages (Fig. 5) indicate that a unit decrease in the 7 days SO_2 flux moving average is significantly associated with an increased probability of having a major explosion. Likewise, a unit decrease in the 7–15-30 days moving averages of the SO_2 concentration is significantly associated with an increased probability of having a major explosion. By contrast, a unit increase in the 7–15-30 days moving average of the CO_2/SO_2 ratio is significantly associated with an increased probability of a major explosion occurring (Fig. 5). Again, no statistically significant association is found for the CO_2 flux, which is not considered further in the analysis below.

Fig. 6a-d illustrates the ROC curves for the variables considered at

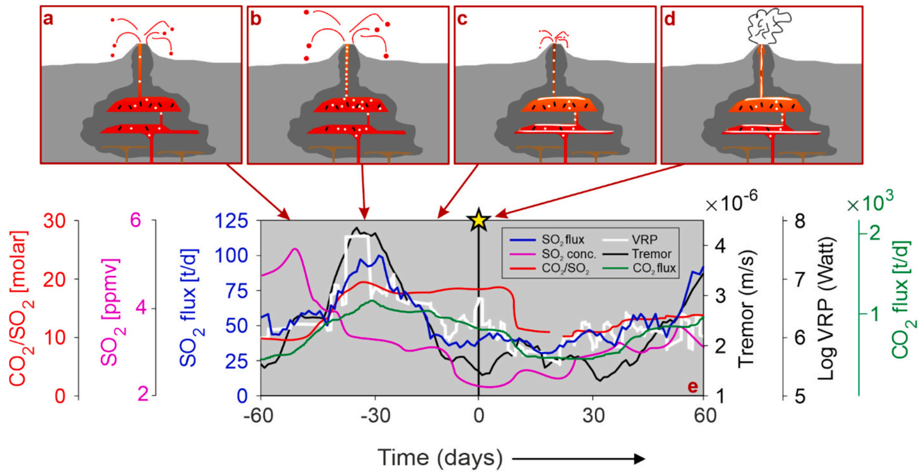

Fig. 9. A simplified, observation based, conceptual models of the sequence of events (a to d) leading to a major explosion. See text. The bottom panel (e) illustrates the temporal evolution of gas (data from Fig. 3b), geophysical (volcanic tremor amplitude; from LGS monitoring network; Ripepe et al., 2009) and thermal output (Volcanic Radiative Power, VRP, from the MIROVA platform, Coppola et al., 2016) records from Stromboli (exemplified by the January to May 2021 event). Time is expressed as days prior to/after the major explosion (set at time = 0).

Lag 3, 7 and 10 days. All considered variables at Lag 3, except for CO_2 concentrations, show moderate ability to predict major explosions (Supplementary Table S6), as evidenced by the AUC >0.5 but <0.7 (Swets, 1988). The AUC of the SO_2 flux is 0.63 (95 % CI: 0.54–0.71) and the optimal threshold (given by the best combination of sensitivity and specificity) is 47 t/d, associated with a 58 % sensitivity and a 61 % specificity. The AUC of the SO_2 concentration is 0.706 (95 % CI: 0.601–0.807), and the optimal threshold is 3.2 ppmv, associated with a 63 % sensitivity and a 71 % specificity. The AUC of the CO_2/SO_2 ratio is 0.67 (95 % CI: 0.53–0.77), and the optimal threshold is 27.8, associated with a 58 % sensitivity and a 69 % specificity. At Lag 7, the CO_2/SO_2 ratio optimal threshold is 26.6, associated with a 66 % sensitivity and a 67 % specificity (Supplementary Table S6). Similar results are obtained using the moving averages at 7, 15 and 30 days (Fig. 6e-f; Supplementary Table S7). 15-days moving average of all considered variables, except for CO_2 concentrations, show moderate ability to predict major eruptions. The AUC of the SO_2 flux is 0.62 (95 % CI: 0.51–0.73) and the optimal threshold is 54 t/d, associated with a 67 % sensitivity and a 54 % specificity. The AUC of the SO_2 concentration is 0.65 (95 % CI: 0.54–0.75), and the optimal threshold is 4.3 ppmv, associated with a 75 % sensitivity and a 57 % specificity. The AUC of the CO_2/SO_2 ratio is 0.66 (95 % CI: 0.57–0.76), and the optimal threshold is 24.7, associated with a 67 % sensitivity and a 59 % specificity (Supplementary Table S6).

The Relative Risks (RRs) obtained using the lagged variables (Fig. 7a-d) show spiky behaviour, except for the CO_2 concentration trend that is flat and uniform throughout the entire observation period. The RRs obtained using the moving averages (Fig. 7e-h) exhibit more well-behaved trends, peaking prior to many of the explosive events.

5. Discussion

5.1. Are gas changes statistically significant?

Our results identify some characteristic patterns in volcanic gas flux/composition time-series prior to Stromboli's major explosions. We find that most major explosions in 2020 to 2023 were preceded by periods (of days to weeks) of reduced plume SO_2 concentrations (highly significant), low SO_2 fluxes and increased CO_2/SO_2 ratios (significant) (Figs. 2, 3). The similar association found for SO_2 fluxes and plume SO_2 concentrations corroborates a causal link between reduced SO_2 and increased eruption likelihood. Analysis shows these variations are statistically significant (*p* values range from 0.002 to 0.02) over temporal timescales of days (Lag 3 in Fig. 4) to weeks (Fig. 5). The same timescales are supported by ROC analysis (Fig. 6), evidencing the repetitive nature of this pattern. Hence, our novel data and analysis provide quantitative statistical validation for the previously reported experimental evidence of a causal link between high CO_2/SO_2 phases and larger-than-ordinary Strombolian explosions at Stromboli found in previous work (Aiuppa et al., 2009, 2010, 2011), yet in which an higher SO_2 concentration threshold was used (relative to the ≥1 ppm level used here and in Aiuppa et al., 2021). In contrast, CO_2 concentrations do not exhibit any statically significant pattern prior to major explosions. We caution that, in addition to reflecting some specific eruption trigger mechanisms (see section 5.3), the low significance of CO_2 concentrations may also result from instrumental limitations. The CO_2-sensing spectrometer has an accuracy of ±2 % of the full scale (3000 ppm in our case), resulting in a ± 60 ppm accuracy. Below 4 ppm SO_2, the median ΔCO_2 is approximately 47 ppm, which is below the sensor's accuracy threshold. This indicates that at low concentrations, the CO_2 sensor may lack sufficient precision to accurately resolve CO_2 levels.

Nearly continuous, long-term records, as those available at Stromboli, are now needed at other persistently active volcanoes (that have a frequent enough eruptive activity) to test the general validity of the statistical association found here. For example, Kunrat et al. (2022) recently applied statistical analysis to SO_2 flux time-series acquired at Sinabung volcano (Indonesia) and found a systematic drop in SO_2 emissions in the 5 days before individual explosions. This case, with the Stromboli example presented here, shows that statistically significant gas changes may be common at volcanoes, and that the paucity of past examples in the literature likely reflects the lack of continuous, long-term gas records at most degassing volcanoes worldwide.

5.2. Evaluating eruption forecast performance

Forecasting volcanic eruptions, a fundamental goal of volcanology (Sparks, 2003), requires that the probability of a future volcanic event is inferred and communicated – together with its associated uncertainty – to governmental authorities and decision makers (Poland and Anderson, 2020). Despite recent major progresses (Acocella et al., 2024), eruption forecasting (deterministic and probabilistic) remains a challenge, especially for sudden, low magnitude (VEI < 3) eruptions (Stix et al., 2023).

Our results can be used to quantitatively evaluate the benefits and limitations of volcanic plume geochemical observations as eruption forecasting tools at Stromboli. To this aim, we combine the Relative Risks (RRs) derived from statistical analysis of the individual gas parameters' time-series (Fig. 7) into a Composite gas indicator (Fig. 8a).

This indicator expresses a gas-based prediction - on a 0 to 1 scale - of having a major explosion, and is based on the linear combination of RRs for the statistically significant moving averages of the SO_2 concentrations (relative weight, 75 %) and CO_2/SO_2 ratios (relative weight, 25 %) (Figs. 5, 6). Notably, although SO_2 concentrations and fluxes are found to have similar association with major explosions (Figs. 3–6), the latter shows less statistical significance than the former. In fact, tests show that inclusion of the SO_2 flux in the Composite indicator reduces its performance (as inferred by the confusion matrix, see below). As discussed previously (Delle Donne et al., 2017, 2022; Lo Bue Trisciuzzi et al., 2024), the currently operating UV camera system offers an incomplete view of the Stromboli's bulk plume, because the plumes issuing from the central and southwestern craters are partially hidden by the northeastern crater ridge. This was found to result in a net underestimation of the total SO_2 flux of ~30 % (Delle Donne et al., 2022; Lo Bue Trisciuzzi et al., 2024). As many of the major explosions studied here were sourced by vents within the central/southwestern crater terrace, we argue that the UV camera may have recurrently failed in capturing in full the pre-explosion drop in SO_2 flux. Additional sources of error do include radiative transfer effects (e.g., plume opacity, light dilution; Kern et al., 2010) that are not accounted for in the current analysis. Based on the results of our statistical analysis, and considering the Multi-GAS units are exposed to emissions from the entire crater terrace, we hence use the SO_2 concentrations as proxy for the volcano SO_2 emissions. The implications of this assumption will be elaborated upon further.

Results (Fig. 8a) show that the Composite indicator varies widely during 2020–2023 (range, 0.08–0.90), and that major explosions are recurrently anticipated by increases to >0.48 (the optimal threshold) days to several weeks beforehand. We evaluate the eruption forecast performance of the indicator from its associated confusion matrix (Fig. 8b), built based on the daily values. This exercise highlights that 19 (TP, True Positives) out of 24 explosions are preceded by increases of the Composite indicator, while 5 are not (FN, False Negatives); hence, the successful prediction rate (100·TP/(TP + FN) =19/24) is 79 %. The same analysis, however, additionally demonstrates a 48 % (100·688/1448) false positive rate (FPR), and a precision (100·TP/(TP + FP) =100·19/707) of only 2.7 %. Finally, the overall correct classification rate (also known as accuracy; expressed by the relationship: 100·(TP + TN)/TOTAL EVENTS = 720/1448) is 52 %. In summary, these results show that our daily geochemical records, although statistically significant (p-value <0.05; Fig. 5), have poor predictive behaviour: daily gas-based alerts would be issued during nearly half of the observation interval, but 97.3 % of them would in fact not be associated with a major explosion.

This analysis presents the challenges we face in estimating and communicating the hazard. First, the true positive alerts enable us to successfully predict the majority of major explosions (19 out of 24 in 2020–2023). Analysis of the five "unpredicted events" indicated that they are among the smallest in size from instrumental viewpoint, e.g., in terms of their associated ground tilt and seismic VLP (Very Long Period) displacement (Ripepe et al., 2021). Tilt and VLP seismicity are explained as due to volumetric expansion of the upper conduit/dyke feeding system, driven by rapid injection of deep gas+magma shortly (minutes to seconds) prior to the blast (Ripepe et al., 2021); hence, their magnitude scales with the volume of gas and/or gas-rich magma that is to erupt. The lower gas volumes of smaller-scale events, in addition to the high level of false positives (see below), may thus justify the lack of any statistically significant pre-bast pattern.

Secondly, it is evident from our analysis that a large fraction (97.3 %) of the gas-based alerts (increases of the Composite indicator; Fig. 8a) would be False positives (e.g., they would not be followed by a major explosion). False positives are especially problematic as they tend to undermine trust of users (decision makers, population) in the monitoring system. In our case, the high false positive rate likely results from the combined action of several factors. Firstly, it is possible that the preparatory gas accumulation phase, as tracked by low SO_2 and high CO_2/SO_2 ratios in the plume, is a necessary but insufficient condition for the explosion: rather, we argue that the accumulated gas can be released passively (e.g., without resulting in an explosion) in most cases. Secondly, the presence of multiple vents with distinct gas compositions (Pering et al., 2020) in the crater terrace may render the plume timeseries noisy, and hence difficult to interpret. Thirdly, and perhaps more importantly, the plume gas concentrations detected by the Multi-GAS units (located at several hundred meters from the degassing vents) are not only modulated by volcanic degassing dynamics, but also by external factors, especially wind speed and direction that govern the extent of plume fumigation at the measurement sites. It is therefore possible that many false positives of the Composite indicator result from low wind speed/unfavourable wind directions, all concurring to determine low SO_2 concentrations. We also cannot exclude that the low SO_2 concentration alerts prior to major explosions are influenced by a combination of volcanological and meteorological effects.

To conclude, when communicating the hazard to authorities, pros and cons of gas observations should be clearly stated. Gas plume monitoring at Stromboli is clearly not yet at a sufficiently mature stage (with the potential of too many false alerts) to be used for daily communicating the hazard of impending major eruptions to authorities with a proper confidence level. Rather than relying on daily acquired data to make inferences on eruption probabilities, a correct use of gas information in decision making should be based on analysing the temporal persistence of anomalous gas changes over longer temporal intervals. We quantitatively explore this possibility by dividing our observational period in 7 day sub-intervals (the weekly averages of the Composite indicator are illustrated in Fig. 8c). Next, we obtain a confusion matrix (Fig. 8d) by analysing the temporal persistence (over a 7 day temporal interval) of the Composite indicator. In this case, we count as True Positives (17) explosions preceded by (at least) 7 consecutive days with above threshold Composite indicator, while False Negatives (7) are explosions that are not preceded by (at least) 7 consecutive days with above threshold Composite indicator (Fig. 8d). With forecasting confined on this 7 day basis, the successful prediction rate (100·TP/(TP + FN) =17/24) decreases to 71 % (relative to 79 % in the previous exercise) but, more importantly, the False Positive rate (FPR = 100·68/209) drastically decreases to ~32 %, and precision (100·TP/(TP + FP) =100*17/85) largely improves to 20 %. The overall correct classification rate (100·134/209) also increases to 64 %. Our results and analysis then confirm that major explosions cluster in prolonged phases (of week(s)) during which the Composite indicator is above threshold (Fig. 8c), and that hence any "guess" of eruption likelihood should be based on longer trends (Fig. 8c) than daily (Fig. 8a).

Access to Stromboli's summit (above 400 m a.s.l.) has been unregulated for years, then regulated (2003–2019) and only recently permanently closed to tourists (2019-present). Access today is limited to monitoring staff personnel since the July 3, 2019 paroxysmal explosion (Giordano and De Astis, 2021). As we wait for research to progress toward the identification of more powerful forecasting tools, to date the gas plume is the only reported mid-term (days to weeks) indicator for an increased likelihood of a major explosion (Fig. 8). Exploiting the capabilities of gas observations - while bearing in mind their caveats and limitations – may enable safer access for volcanologists and monitoring staff.

5.3. Implications for the driving mechanisms of major explosions

Our observations (Figs. 2, 3) and analyses (Figs. 4–6) also offer novel pieces of information to understand the driving mechanisms of sudden basaltic explosions. These relatively small (VEI < 1) but hazardous blasts are not unique to Stromboli (where they are referred as "major explosions" and "paroxysms", based on their intensity/magnitude), but rather common to open-vent basaltic volcanoes globally (Vergniolle and Métrich, 2022). Owing to their characteristics, such as sudden initiation, short duration (seconds to minutes) and unsteady (unsustained column) behaviour, these blasts are generally thought to be driven by the catastrophic release of accumulated and pressurized volatiles (Stix et al., 2023); however, the processes responsible for driving the volcano to such a critical state can be variable in space and time, and include both bottom-up and top-down mechanisms (Stix et al., 2023).

At Stromboli, paroxysms have typically been explained as triggered by the fast ascent of either gas (Allard, 2010) or gas-rich magma (Métrich et al., 2001, 2010, 2021) from the deep magma plumbing system (bottom-up mechanism), but examples of top-bottom mechanisms, in which paroxysms are favoured by rapid decompression of deep-seated magma by shallow conduit emptying (caused by lateral lava effusion), also exist (Aiuppa et al., 2010; Aiuppa et al., 2021; Calvari et al., 2011; Ripepe et al., 2015). Conflicting views also exist for major explosions, since resolving between top-bottom (Falsaperla and Spampinato, 2003; Calvari et al., 2012) vs. bottom-up (Andronico and Pistolesi, 2010; Pioli et al., 2014; Voloschina et al., 2023) processes is complicated by more controversial geochemical/petrological evidence (erupted materials are heterogeneous mixtures of denser/degassed stored conduit magma fragments and vesicular/crystal-poor deeper LP magma fragments; see discussion in Voloschina et al., 2023 and Insinga et al., 2024).

One key point here is that our statistical analysis finds no systematic temporal association between major explosions and CO_2 concentrations/fluxes (Figs. 4a, 5, 6, 7c, g). Owing to very low solubility in silicate melts, shallow stored magma is typically extremely depleted in CO_2 (Edmonds and Wallace, 2017). Hence, increasing CO_2 emissions at open-vent volcanoes (Aiuppa et al., 2010; Edmonds et al., 2022) have characteristically been interpreted as caused by precursory CO_2-rich gas bubble leakage from deeply stored, mafic magma, and hence evidence of a bottom-up eruption mechanism. At Stromboli, increasing CO_2 concentrations and fluxes in the weeks/months prior to the July 3, 2019 paroxysm (Supplementary Figure S3; Aiuppa et al., 2021) have been explained by progressive bubble accumulation into, and passive leakage from, deeply stored LP magma, ultimately causing pressure build-up at depth, and LP magma ascent and eruption. Of the 2020–2023 major explosions studied here, only the July 2020 explosion, the largest of this class of events in terms of geophysical (tilt and VLP; Ripepe et al., 2021) and volcanological (Voloschina et al., 2023) parameters, is associated with a CO_2 concentration increase similar, or even larger, than that observed prior to the July 2019 paroxysm (Supplementary Fig. S3). This, in combination with the CO_2 flux increase (Fig. 2f and Voloschina et al., 2023), points to a bottom-up mechanism for the July 2020 event (and potentially for a few others in 2009, Aiuppa et al., 2011; Insinga et al., 2024). However, the lack of any distinctive CO_2 concentration/flux trend for the remaining 2020–2023 explosions (Fig. 2), and the generally lower CO_2 fluxes relative to those observed in concomitance with the 2019 events (Supplementary Fig. S3), require a distinct mechanism.

Our analysis shows that the pre-major explosion CO_2/SO_2 ratio increases in 2020–2023 (Figs. 4–6) are systematically caused by decreasing SO_2 concentrations (Figs. 4, 5) rather than increasing CO_2 concentrations. Major explosions are also systematically clustered in periods of reduced SO_2 fluxes (Figs. 2–7; although with the limitations discussed above). This association is especially intriguing as the SO_2 flux is a proxy for the volume of magma that is ascending (and degassing) in the topmost ~3–4 km of the Stromboli's magma feeding system (Allard et al., 1994; Laiolo et al., 2022). Hence, the recurrent (Figs. 2–3) drop in SO_2 concentrations/fluxes prior to most of Stromboli's major explosions is suggestive of a process in which slowing down of shallow magma circulation (acting over timescales of days to weeks) creates the favorable conditions for major explosions to occur.

Our preferred hypothesis of a top-down control on major explosions is schematically illustrated in Fig. 9. This simplified model, exemplified by the gas observations taken in January–May 2021 (Fig. 3b), also builds on temporal records of (i) volcanic tremor amplitude (data from the Laboratorio Geofisica Sperimentale, UniFi network: Ripepe et al., 2009) and (ii) thermal output (as based on estimates of Volcanic Radiative Power obtained from infrared satellite data; Coppola et al., 2016). These two parameters are typically used to parametrize the level of activity of the shallow magmatic column at Stromboli, and they consistently increase when gas-rich, more buoyant magma circulates in the volcano's upper magma feeding system, hence sustaining more vigorous regular (Strombolian) activity (e.g., Valade et al., 2016), and decrease when the shallow gas±magma supply is reduced.

In our hypothesis, regular Strombolian activity (panels a and b) is fed by sustained circulation and degassing of magma in the upper conduit/dyke feeding system (Allard et al., 2008). The convecting magma column is relatively permeable to deeply sourced gas bubbles. If the upper feeding system is increasingly percolated (Burton et al., 2007) by deeply-sourced bubbles (panel b), as tracked by increasing CO_2 fluxes (panel e), Strombolian activity intensifies, volcanic tremor amplitude increases (because of an increased gas bubble coalescence and bursting; Ripepe and Gordeev, 1999), and SO_2 flux and thermal output (VRP) concurrently increase because bubbly magma is more buoyant and faster convecting, releasing more gas and heat to the surface (Laiolo et al., 2022). With time, however, flushing by deeply sourced (CO_2-rich) gas causes the shallow resident magma to dehydrate, to become more viscous and stagnant (Caricchi et al., 2024). This slowing down of the upper magma column (panel c) causes a waning of Strombolian activity, as tracked by decreasing seismic and thermal activity, and by declining SO_2 and CO_2 fluxes. Notably, the CO_2/SO_2 ratio remains high in this phase (c). We propose that the viscous magma acts as a rheological (permeability) barrier below which deep gas bubbles can accumulate. If so, the high CO_2/SO_2 ratios in phase (c) would result from a combination of ineffective SO_2 release from the stagnant (degassed) magma column (see decreasing SO_2 fluxes and concentrations) and passive leakage of some accumulated gas (Aiuppa et al., 2021), as corroborated by the CO_2 flux decreasing less than the SO_2 flux (panel e). The depth of the gas accumulation zone (the base of the rheological barrier) is difficult to constrain. However, the CO_2/SO_2 ratios of >23.6–31 that are statistically recorded in the run-up (3–15 days prior) to the "predicted" major explosions (Fig. 8) imply source depths of ~2–4 km below the summit vents (based on the modelled pressure dependence of the magmatic gas CO_2/SO_2 ratio at Stromboli; Aiuppa et al., 2021). If this interpretation is correct, then the "unpredicted" 2020–2023 major explosions (Fig. 8) may reflect shallower gas accumulation, a condition where the accumulated gas bubbles would have CO_2/SO_2 ratio unresolvable from background (passive) degassing. The fact these 5–7 events (Fig. 8) are volumetrically less important (based on geophysical evidence) supports this shallower origin. Ultimately, as some overpressure level is reached, catastrophic release and rise of previously accumulated gas (± some deep LP magma) takes place during one (or in a sequence of) major explosion(s) (panel d). Removal of viscous stagnant magma (as HP magma fragments) in the major explosion(s) re-establishes permeable gas flow and active magma circulation in the upper conduit/feeding dyke, ultimately rejuvenating Strombolian activity (return to phase a).

We caution that this model is only based on observational evidence (Fig. 9), while quantitative (fluid-dynamic) modeling would be needed to critically test its feasibility. Nevertheless, the mid-term (days/weeks) feedback mechanism between the shallow and deep portions of Stromboli's magma plumbing system it is based upon explains well the temporal fluctuations in regular (Strombolian) activity (Ripepe et al., 2008), the clustering of major explosions in sequences of closely spaced events (Fig. 2a), and their concentration in periods of reduced shallow degassing activity (Fig. 9).

6. Conclusions

The statistical significance of plume compositional/flux records as potential forecasting tools of sudden, larger-than-normal (major) explosions at Stromboli has been tested. Our results and analyses identify a recurrent volcanic gas temporal pattern prior to Stromboli's major explosions (in 2020–2023), in which these events are statistically preceded (over timescales of days to weeks) by: (i) low SO_2 concentrations and fluxes and (ii) high CO_2/SO_2 ratios. We have integrated these results into a gas-based Composite indicator, from which we obtain a success prediction rate (as expressed by the TPR) of 71 % on a weekly basis (e.g., by counting the number of explosions preceded by above threshold Composite indicator for at least 7 consecutive days). The TPR increases to 79 % if daily values of the compositive indicator are used instead (but precision is only 2.7 % in this case). The weekly Composite indicator, based on the weighted linear combination of statistically significant parameters (SO_2 concentrations and CO_2/SO_2 ratios), can be implemented in real-time from monitoring data and, if additionally tested and improved to improve the currently low precision (20 %), may evolve into a potentially exploitable monitoring and decision-making tool in the future.

We interpret these variations in view of a top-down mechanism (Fig. 9), in which: (a) convective overturning of shallow magma in the feeding conduit/dyke system slows down (potentially due to the dehydration effect of CO_2 flushing; Caricchi et al., 2024), causing (b) gas bubbles to accumulate below a rheological discontinuity (the base of the viscous plug, formed by stagnant shallow HP magma), and hence (c) the catastrophic release of accumulated gas (plus a mixture of some deep LP magma and fragments of the HP magma plug) in a (or sequence of) major explosion(s). We stress that our results do not preclude other driving mechanisms for major explosions. For example, a bottom-up mechanism involving ascent of mafic LP magma from depth has been identified on a petrological basis for the July 19, 2020, major explosion (Voloschina et al., 2023). This event consistently exhibits the most evident ΔCO_2 variation (Figs. 2, 7g) in our dataset, and fails to be "predicted" by our Composite indicator (Fig. 8), suggesting a distinct source mechanism. This is in agreement with its larger magnitude and with petrological and geophysical characteristics almost overlapping with those of paroxysmal eruptions at Stromboli.

One very critical aspect to consider is that, as noted, our Composite indicator is associated with a high (32 %) false positive rate and hence low precision, which limits its applicability as an operational forecasting tool (at least in its present form). Identifying new processing tools and/or new parameters that can more effectively monitor overpressure development in the explosion generation zone is critical to more robust forecasting of the small scale (VEI $<$ 1) class of eruptions studied here. For example, use of artificial intelligence (machine learning) is now under test to identify any hidden pattern in our dataset. A second UV camera system has been recently deployed at Stromboli to mitigate against incomplete coverage of the bulk plume by the currently operating UV camera system (Lo Bue Trisciuzzi et al., 2024). New data processing tools are being explored to filter out from the Multi-GAS dataset observational periods with wind speed/direction unsuitable for plume fumigation at the measurement sites (Tamburello et al., 2023). Hopefully, this expanded dataset and analysis will help reducing the currently high false positive rate.

Ultimately, it is important to recall that Stromboli's major explosions rank at the lower end of the range of volcanic explosive eruptions and better eruption forecasting success rates are expected for larger-scale explosive events (Aiuppa et al., 2021; Acocella et al., 2024).

CRediT authorship contribution statement

Alessandro Aiuppa: Writing – original draft, Visualization, Supervision, Project administration, Methodology, Investigation, Funding acquisition, Formal analysis, Data curation, Conceptualization. **Marcello Bitetto:** Methodology, Investigation, Data curation. **Luciano Curcio:** Methodology, Investigation, Data curation. **Dario Delle Donne:** Writing – review & editing, Validation, Software, Methodology, Formal analysis. **João Lages:** Methodology, Investigation, Data curation. **Giovanni Lo Bue Trisciuzzi:** Visualization, Software, Methodology, Investigation, Formal analysis. **Giancarlo Tamburello:** Writing – review & editing, Software, Methodology, Investigation, Formal analysis, Data curation. **Angelo Vitale:** Methodology, Investigation, Data curation. **Flavio Cannavò:** Writing – review & editing, Methodology, Investigation. **Mauro Coltelli:** Writing – review & editing, Project administration, Funding acquisition. **Diego Coppola:** Writing – review & editing, Methodology, Investigation, Data curation. **Lorenzo Innocenti:** Visualization, Resources, Methodology, Data curation. **Laura Insinga:** Methodology, Investigation. **Giorgio Lacanna:** Writing – review & editing, Methodology, Investigation. **Marco Laiolo:** Writing – review & editing, Methodology, Investigation, Data curation. **Francesco Massimetti:** Methodology, Investigation, Data curation. **Marco Pistolesi:** Writing – review & editing, Methodology, Investigation. **Eugenio Privitera:** Project administration, Methodology, Investigation, Funding acquisition. **Maurizio Ripepe:** Writing – review & editing, Methodology, Investigation. **Marija Voloschina:** Methodology, Writing – review & editing, Investigation. **Giovanna Cilluffo:** Writing – review & editing, Visualization, Validation, Software, Methodology, Investigation, Formal analysis.

Declaration of competing interest

The authors declare that they have no known competing financial interests or personal relationships that could have appeared to influence the work reported in this paper.

Acknowledgements

This study received funding through the service activity enhancement project "Sviluppo del sistema unico (INGV-Università) di monitoraggio vulcanico e rilevamento precoce dei maremoti e delle esplosioni parossistiche di Stromboli"funded by the Dipartimento della Protezione Civile and the INGV. The study/service/product does not necessarily reflect the policy and position of the Istituto Nazionale di Geofisica e Vulcanologia and Dipartimento della Protezione Civile, Italy. Funding was also made available by the RETURN Extended Partnership funded by the European Union Next-GenerationEU (National Recovery and Resilience Plan – NRRP, Mission 4, Component 2, Investment 1.3 – D.D. 1243 2/8/2022, PE0000005). The authors wish to thank Glyn Williams-Jones and one anonymous reviewer for useful comments on an earlier version of the manuscript.

Appendix A. Supplementary data

Supplementary data to this article can be found online at https://doi.org/10.1016/j.jvolgeores.2025.108325.

Data availability

All data provided as electronic supplement

References

Acocella, V., Ripepe, M., Rivalta, E., et al., 2024. Towards scientific forecasting of magmatic eruptions. Nat. Rev. Earth Environ. 5, 5–22. https://doi.org/10.1038/s43017-023-00492-z.

Aiuppa, A., Moretti, R., Federico, C., Giudice, G., Gurrieri, S., Liuzzo, M., et al., 2007. Forecasting Etna eruptions by real time evaluation of volcanic gas composition. Geology 35 (12), 1115–1118. https://doi.org/10.1130/G24149A.

Aiuppa, A., Federico, C., Giudice, G., Giuffrida, G., Guida, R., Gurrieri, S., Liuzzo, M., Moretti, R., Papale, P., 2009. The 2007 eruption of Stromboli volcano: insights from real-time measurements of the volcanic gas plume CO_2/SO_2 ratio. J. Volcanol. Geotherm. Res. 182, 221–230.

Aiuppa, A., et al., 2010. Unusually large magmatic CO_2 gas emissions prior to a basaltic paroxysm. Geophys. Res. Lett. 37 (17) (art. no. L17303).

Aiuppa, A., Burton, M., Allard, P., Caltabiano, T., Giudice, G., Gurrieri, S., Liuzzo, M., Salerno, G., 2011. First observational evidence for the CO_2-driven origin of Stromboli's major explosions. Solid Earth 2 (2), 135–142. https://doi.org/10.5194/se-2-135-2011.

Aiuppa, A., et al., 2017. CO_2-gas precursor to the March 2015 Villarrica volcano eruption. Geochem. Geophys. Geosyst. 18 (6), 2120–2132. https://doi.org/10.1002/2017GC006892.

Aiuppa, A., et al., 2018. Tracking Formation of a Lava Lake From Ground and Space: Masaya Volcano (Nicaragua), 2014–2017. Geochem. Geophys. Geosyst. 19 (2), 496–515. https://doi.org/10.1002/2017GC007227.

Aiuppa, A., Bitetto, M., Delle Donne, D., La Monica, F.P., Tamburello, G., Coppola, D., et al., 2021. Volcanic CO_2 tracks the incubation period of basaltic paroxysms. Sci. Adv. 7 (38). https://doi.org/10.1126/sciadv.abh0191.

Aiuppa, A., Lo Bue Trisciuzzi, G., Alparone, S., Bitetto, M., Coltelli, M., Delle Donne, D., Ganci, G., Pecora, E., 2023. A SO_2 flux study of the Etna volcano 2020–2021 paroxysmal sequences. Front. Earth Sci. 11, 1115111. https://doi.org/10.3389/feart.2023.1115111.

Allard, P., 2010. A CO_2-rich gas trigger of explosive paroxysms at Stromboli basaltic volcano, Italy. J. Volcanol. Geotherm. Res. 189 (3–4), 363–374. https://doi.org/10.1016/j.jvolgeores.2009.11.018.

Allard, P., Carbonnelle, J., Métrich, N., Loyer, H., Zettwoog, P., 1994. Sulphur output and magma degassing budget of Stromboli volcano. Nature 368, 326–330. https://doi.org/10.1038/368326a0.

Allard, P., Aiuppa, A., Burton, M., Caltabiano, T., Federico, C., Salerno, G., La Spina, A., 2008. Crater gas emissions and the magma feeding system of Stromboli volcano. In: Calvari, S., Inguaggiato, S., Puglisi, G., Ripepe, M., Rosi, M. (Eds.), Learning from Stromboli: AGU Geophysics Monograph Series, 182, pp. 65–80. Washington DC.

Andronico, D., Pistolesi, M., 2010. The November 2009 paroxysmal explosions at Stromboli. J. Volcanol. Geotherm. Res. 196, 120–125. https://doi.org/10.1016/j.jvolgeores.2010.06.005.

Arellano, S., et al., 2021. Synoptic analysis of a decade of daily measurements of SO_2 emission in the troposphere from volcanoes of the global ground-based network for observation of volcanic and atmospheric change. Earth Syst. Sci. Data 13, 1167–1188. https://doi.org/10.5194/essd-13-1167-2021.

Bennett, D.A., 2001. How can I deal with missing data in my study? Aust NZ J Public Health 25 (5), 464–469.

Bertagnini, A., Coltelli, M., Landi, P., et al., 1999. Violent explosions yield new insights into dynamics of Stromboli volcano. Eos (Washington DC) 80, 2–8. https://doi.org/10.1029/99EO00415.

Bevilacqua, A., Bertagnini, A., Pompilio, M., et al., 2020. Major explosions and paroxysms at Stromboli (Italy): a new historical catalog and temporal models of occurrence with uncertainty quantification. Sci. Rep. 10, 1–18. https://doi.org/10.1038/s41598-020-74301-8.

Biggs, J., Pritchard, M.E., 2017. Global volcano monitoring: what does it mean when volcanoes deform? Elements 13 (1), 17–22. https://doi.org/10.2113/gselements.13.1.17.

Bonaccorso, A., Caltabiano, T., Currenti, G., Del Negro, C., Gambino, S., Ganci, G., Giammanco, S., Greco, F., Pistorio, A., Salerno, G., Spampinato, S., Boschi, E., 2011. Dynamics of a lava fountain revealed by geophysical, geochemical and thermal satellite measurements: the case of the 10 April 2011 Mt Etna eruption. Geophys. Res. Lett. 38. https://doi.org/10.1029/2011GL049637.

Brandsdóttir, B., Einarsson, P., 1992. Volcanic Tremor and Low-Frequency Earthquakes in Iceland. In: Gasparini, P., Scarpa, R., Aki, K. (Eds.), Volcanic Seismology, IAVCEI Proceedings in Volcanology. Springer, Berlin Heidelberg, Berlin, Heidelberg, pp. 212–222. https://doi.org/10.1007/978-3-642-77008-1_16.

Burton, M.R., Mader, H.M., Polacci, M., 2007. The role of gas percolation in quiescent degassing of persistently active basaltic volcanoes. Earth Planet. Sci. Lett. 264, 46–60.

Burton, M.R., Caltabiano, T., Murè, F., Salerno, G., Randazzo, D., 2009. SO_2 flux from Stromboli during the 2007 eruption: results from the FLAME network and traverse measurements. J. Volcanol. Geotherm. Res. 182, 214–220. https://doi.org/10.1016/j.jvolgeores.2008.11.025.

Calvari, S., Spampinato, L., Bonaccorso, A., Oppenheimer, C., Rivalta, E., Boschi, E., 2011. Lava effusion-a slow fuse for paroxysms at Stromboli volcano? Earth Planet. Sci. Lett. 301 (1–2), 317–323. https://doi.org/10.1016/j.epsl.2010.11.015.

Calvari, S., Büttner, R., Cristaldi, A., et al., 2012. The 7 September 2008 Vulcanian explosion at Stromboli volcano: multiparametric characterization of the event and quantification of the ejecta. J. Geophys. Res. Solid Earth 117, 1–17. https://doi.org/10.1029/2011JB009048.

Campus, A., Laiolo, M., Massimetti, F., Coppola, D., 2022. (2022) the transition from MODIS to VIIRS for Global Volcano thermal monitoring. Sensors 22, 1713. https://doi.org/10.3390/s22051713.

Caricchi, L., Montagna, C.P., Aiuppa, A., Lages, J., Tamburello, G., Papale, P., 2024. CO_2 flushing triggers paroxysmal eruptions at open conduit basaltic volcanoes. J. Geophys. Res. Solid Earth 129. https://doi.org/10.1029/2023JB028486.

Chouet, B., Saccorotti, G., Martini, M., Dawson, P., De Luca, G., Milana, G., Scarpa, R., 1997. Source and path effects in the wave fields of tremor and explosions at Stromboli Volcano, Italy. J. Geophys. Res. 102, 15129–15150. https://doi.org/10.1029/97JB00953.

Cilluffo, G., et al., 2024. A comprehensive environmental exposure indicator and respiratory health in asthmatic children: a case study. Environ. Ecol. Stat. 1–19.

Coppola, D.; Laiolo, M. Delle Donne, D. Ripepe, M., Cigolini, C. (2014). Hot-spot detection and characterization of strombolian activity from MODIS infrared data. Int. J. Remote Sens., vol. 35(9), p. 3403–3426. doi:https://doi.org/10.1080/01431161.2014.903354.

Coppola, D., Laiolo, M., Cigolini, C., Delle Donne, D., Ripepe, M., 2016. Enhanced volcanic hot-spot detection using MODIS IR data: Results from the MIROVA system. In: Harris, A.J.L., De Groeve, T., Garel, F., Carn, S.A. (Eds.), Detecting, Modelling, and Responding to Effusive Eruptions. In: Geological Society. Special Publications, London.

Coppola, D., Cardone, D., Laiolo, M., Aveni, S., Campus, A., Massimetti, F., 2023. Global radiant flux from active volcanoes: the 2000-2019 MIROVA Database. Front. Earth Sci. 11, 1240107. https://doi.org/10.3389/feart.2023.1240107.

de Moor, J.M., et al., 2016a. Turmoil at Turrialba Volcano (Costa Rica): Degassing and eruptive processes inferred from high-frequency gas monitoring. J. Geophys. Res. Solid Earth 121 (8), 5761–5775. https://doi.org/10.1002/2016JB013150.

de Moor, J.M., Aiuppa, A., Pacheco, J., Avard, G., Kern, C., Liuzzo, M., Martínez, M., Giudice, G., Fischer, T.P., 2016b. Short-period volcanic gas precursors to phreatic eruptions: Insights from Poás Volcano, Costa Rica. Earth Planet. Sci. Lett. 442, 218–227. https://doi.org/10.1016/j.epsl.2016.02.056.

de Moor, J.M., Stix, J., Avard, G., Muller, C., Corrales, E., Diaz, J.A., Alan, A., Brenes, J., Pacheco, J., Aiuppa, A., Fischer, T.P., 2019. Insights on hydrothermal-magmatic interactions and eruptive processes at Poás Volcano (Costa Rica) from high-frequency gas monitoring and drone measurements. Geophys. Res. Lett. 46 (3), 1293–1302. https://doi.org/10.1029/2018GL080301.

Delle Donne, D., Tamburello, G., Aiuppa, A., Bitetto, M., Lacanna, G., D'Aleo, R., Ripepe, M., 2017. Exploring the explosive-effusive transition using permanent ultraviolet cameras. J. Geophys. Res. Solid Earth 122, 4377–4394. https://doi.org/10.1002/2017JB014027.

Delle Donne, D., Lo Coco, E., Bitetto, M., La Monica, F.P., Lacanna, G., Lages, J., Ripepe, M., Tamburello, G., Aiuppa, A., 2022. Spatio-temporal changes in degassing behavior at Stromboli volcano derived from two co-exposed SO2 camera stations. Front. Earth Sci. 10. https://doi.org/10.3389/feart.2022.972071 art. no. 972071.

DeLong, E.R., DeLong, D.M., Clarke-Pearson, D.L., 1988. Comparing the areas under two or more correlated receiver operating characteristic curves: a nonparametric approach. Biometrics 44 (03), 837–845.

Edmonds, M., 2021. Geochemical monitoring of volcanoes and the mitigation of volcanic gas hazards. In: Papale, P. (Ed.), Hazards and Disasters Series, Forecasting and Planning for Volcanic Hazards, Risks, and Disasters, vol. 2. Elsevier. https://doi.org/10.1016/B978-0-12-818082-2.09995-9.

Edmonds, M., Wallace, P.J., 2017. Volatiles and exsolved vapor in volcanic systems. Elements 13 (1), 29–34. https://doi.org/10.2113/gselements.13.1.29.

Edmonds, M., Oppenheimer, C., Pyle, D.M., Herd, R.A., Thompson, G., 2003. SO_2 emissions from Soufrière Hills Volcano and their relationship to conduit permeability, hydrothermal interaction and degassing regime. J. Volcanol. Geotherm. Res. 124, 23–43. https://doi.org/10.1016/S0377-0273(03)00041-6.

Edmonds, M., Liu, E.J., Cashman, K.V., 2022. Open-vent volcanoes fuelled by depth-integrated magma degassing. Bull. Volcanol. 84, 28.

Falsaperla, S., Spampinato, S., 2003. Seismic insight into explosive paroxysms at Stromboli volcano, Italy. J. Volcanol. Geotherm. Res. 125, 137–150.

Federico, C., Inguaggiato, S., Liotta, M., Rizzo, A.L., Vita, F., 2023. Decadal monitoring of the Hydrothermal System of Stromboli Volcano, Italy. Geochem. Geophys. Geosyst. 24 (9). https://doi.org/10.1029/2023GC010931 art. no. e2023GC010931.

Fischer, T.P., Morrissey, M.M., Marta Lucía Calvache, V., Diego Gòmez, M., Roberto Torres, C., Stix, J., Williams, S.N., 1994. Correlations between SO_2 flux and long-period seismicity at Galeras volcano. Nature 368, 135–137. https://doi.org/10.1038/368135a0.

Giordano, G., De Astis, G., 2021. The summer 2019 basaltic Vulcanian eruptions (paroxysms) of Stromboli. Bull. Volcanol. 83, 1.

Global Volcanism Program, 2023. Report on Stromboli (Italy). In: Bennis, K.L., Venzke, E. (Eds.), Bulletin of the Global Volcanism Network, vol. 48. Smithsonian Institution, p. 2.

Gordeev, E.I., (1993) Modeling of volcanic tremor as explosive point sources in a singled-layered, elastic half-space, J. Geophys. Res., 98, 19,687–19,703.

Inguaggiato, S., Jácome Paz, M.P., Mazot, A., Delgado Granados, H., Inguaggiato, C., Vita, F., 2013. CO_2 output discharged from Stromboli Island (Italy) (2013). Chem. Geol. 339, 52–60. https://doi.org/10.1016/j.chemgeo.2012.10.008.

Inguaggiato, S., Vita, F., Cangemi, M., Mazot, A., Sollami, A., Calderone, L., Morici, S., Jacome Paz, M.P., 2017. Stromboli volcanic activity variations inferred from observations of fluid geochemistry: 16 years of continuous monitoring of soil CO_2 fluxes (2000–2015). Chem. Geol. 469, 69–84. https://doi.org/10.1016/j.chemgeo.2017.01.030.

Insinga, L., Voloschina, M., Marianelli, P., et al., 2024. Constraints on magma source, pre-eruptive dynamics and timescales of the 2009 major explosions at Stromboli volcano (Italy). Proc. 6th Rittmann Conference, Catania, Settembre 2024. Miscellanea INGV 83, 166–167.

Kern, C., Deutschmann, T., Vogel, L., Wöhrbach, M., Wagner, T., Platt, U., 2010. Radiative transfer corrections for accurate spectroscopic measurements of volcanic gas emissions. Bull. Volcanol. 72, 233–247. https://doi.org/10.1007/s00445-009-0313-7.

Kern, C., Aiuppa, A., de Moor, J.M., 2022. (2022) a golden era for volcanic gas geochemistry? Bull. Volcanol. 84, 43. https://doi.org/10.1007/s00445-022-01556-6.

Kunrat, S., Kern, C., Alfianti, H., Lerner, A.H., 2022. Forecasting explosions at Sinabung Volcano, Indonesia, based on SO_2 emission rates. Front. Earth Sci. 10, 976928. https://doi.org/10.3389/feart.2022.976928.

La Felice, S., Landi, P., 2011. The 2009 paroxysmal explosions at Stromboli (Italy): magma mixing and eruption dynamics. Bull. Volcanol. 73, 1147–1154. https://doi.org/10.1007/s00445-011- 0502-z.

Laiolo, M., Delle Donne, D., Coppola, D., Bitetto, M., Cigolini, C., Della Schiava, M., et al., 2022. Shallow magma dynamics at open-vent volcanoes tracked by coupled thermal and SO_2 observations. Earth Planet. Sci. Lett. 594, 117726. https://doi.org/10.1016/j.epsl.2022.117726.

Landi, P., Métrich, N., Bertagnini, A., Rosi, M., 2008. Recycling and "rehydration" of degassed magma inducing transient dissolution/crystallization events at Stromboli (Italy). J. Volcanol. Geotherm. Res. 174, 325–336. https://doi.org/10.1016/j.jvolgeores.2008.02.013.

Lo Bue Trisciuzzi, G., Aiuppa, A., Salerno, G., et al., 2024. Improved volcanic SO_2 flux records from integrated scanning-DOAS and UV Camera observations. J. Volcanol. Geotherm. Res. 455. https://doi.org/10.1016/j.jvolgeores.2024.108207.

Logan, J.A., 1983. A multivariate model for mobility tables. Am. J. Sociol. 89, 324–349.

Massimetti, F., Laiolo, M., Aiuppa, A., Aveni, S., Bitetto, M., Campus, A., Coltelli, M., Cristaldi, A., Donne, D.D., Innocenti, L., Lacanna, G., Pistolesi, M., Privitera, E., Ripepe, M., Salerno, G., Coppola, D., 2024. Thermal Emissions of active Craters at Stromboli Volcano: Spatio-Temporal Insights from 10 years of Satellite Observations. J. Gemophys. Res. Solid Earth 129 (9). https://doi.org/10.1029/2024JB029143 e2024JB029143.

Matoza, R.S., Roman, D.C., 2022. (2022) one hundred years of advances in volcano seismology and acoustics. Bull. Volcanol. 84, 86. https://doi.org/10.1007/s00445-022-01586-0.

McNutt, S.R., 2002. Volcano seismology and monitoring for eruptions. In: International Geophysics. Elsevier. https://doi.org/10.1016/S0074-6142(02)80228-5, pp. 383–V.

McNutt, S.R., Nishimura, T., 2008. Volcanic tremor during eruptions: Temporal characteristics, scaling and constraints on conduit size and processes. J. Volcanol. Geotherm. Res. 178 (1), 10–18. https://doi.org/10.1016/j.jvolgeores.2008.03.010.

Menyailov, I.A., 1975. Prediction of eruptions using changes in compositions of volcanic gases. Bull. Volcanol. 39, 112–125.

Métrich, N., Bertagnini, A., Landi, P., Rosi, M., 2001. Crystallization driven by decompression and water loss at Stromboli volcano (Aeolian Islands, Italy). J. Petrol. 42, 1471–1490. https://doi.org/10.1093/petrology/42.8.1471.

Métrich, N., Bertagnini, A., di Muro, A., 2010. Conditions of magma storage, degassing and ascent at Stromboli: New insights into the volcano plumbing system with inferences on the eruptive dynamics. J. Petrol. 51, 603–626. https://doi.org/10.1093/petrology/egp083.

Métrich, N., Bertagnini, A., Pistolesi, M., 2021. Paroxysms at Stromboli volcano (Italy): source, genesis and dynamics. Front. Earth Sci. 9, 1–17. https://doi.org/10.3389/feart.2021.593339.

Nadeau, P.A., Werner, C.A., Waite, G.P., Carn, S.A., Brewer, I.D., Elias, T., Sutton, A.J., Kern, C., 2015. Using SO_2 camera imagery and seismicity to examine degassing and gas accumulation at Kīlauea Volcano, May 2010. J. Volcanol. Geotherm. Res. 300, 70–80. https://doi.org/10.1016/j.jvolgeores.2014.12.005.

Oppenheimer, C., Fischer, T.P., Scaillet, B., 2014. Volcanic degassing: process and impact. In: Holland, H.D., Turekian, K.K. (Eds.), Treatise on Geochemistry, 2nd ediion. Elsevier, Amsterdam, pp. 111–179. https://doi.org/10.1016/B978-0-08-095975-7.00304-1.

Papale, P., Moretti, R., Paonita, P., 2022. Thermodynamics of multi-component gas–melt equilibrium in magmas: theory, models, and applications. Rev. Mineral. Geochem. 87-1, 431–556.

Patanè, D., Aiuppa, A., Aloisi, M., Behncke, B., Cannata, A., Coltelli, M., Di Grazia, G., Gambino, S., Gurrieri, S., Mattia, M., Salerno, G., 2013. Insights into magma and fluid transfer at Mount Etna by a multiparametric approach: a model of the events leading to the 2011 eruptive cycle. JGR Solid Earth 118, 3519–3539. https://doi.org/10.1002/jgrb.50248.

Pering, T.D., Liu, E.J., Wood, K., Wilkes, T.C., Aiuppa, A., Tamburello, G., Bitetto, M., Richardson, T., McGonigle, A.J.S., 2020. Composite ground and aerial measurements resolve vent-specific gas fluxes from a multi-vent volcano. Nat. Commun. 11 (1). https://doi.org/10.1038/s41467-020-16862-w art. no. 3039.

Pichavant, M., di Carlo, I., Le Gac, Y., Rotolo, S.G., Scaillet, B., 2009. Experimental constraints on the deep magma feeding system at Stromboli Volcano, Italy. J. Petrol. 50 (4), 601–624. https://doi.org/10.1093/petrology/egp014.

Pichavant, M., Di Carlo, I., Pompilio, M., le Gall, N., 2022. Timescales and Mechanisms of Paroxysm Initiation at Stromboli Volcano. Italy Bullet Volcanol, Aeolian Islands. https://doi.org/10.1007/s00445-022-01545-9.

Pioli, L., Pistolesi, M., Rosi, M., 2014. Transient explosions at open-vent volcanoes: the case of Stromboli (Italy). Geology 3–6. https://doi.org/10.1130/G35844.1.

Poland, M.P., Anderson, K.R., 2020. Partly cloudy with a chance of lava flows: forecasting volcanic eruptions in the twenty-first century. J. Geophys. Res. Solid Earth 125 e2018JB016974.

Reath, K., et al., 2019. Thermal, deformation, and degassing remote sensing time series (CE 2000–2017) at the 47 most active volcanoes in Latin America: implications for volcanic systems. J. Geophys. Res. Solid Earth 124, 195–218.

Ripepe, M., Gordeev, E., 1999. Gas bubble dynamics model for shallow volcanic tremor at Stromboli. J. Geophys. Res. 104, 10,639–10,654. https://doi.org/10.1029/98JB02734.

Ripepe, M., Poggi, P., Braun, T., Gordeev, E., 1996. Infrasonic waves and volcanic tremor at Stromboli. Geophys. Res. Lett. 23, 181–184.

Ripepe, M., Delle, Donne D., Harris, A., Marchetti, E., Ulivieri, G., 2008. Dynamics of Strombolian activity. In: Calvari, S., Inguaggiato, S., Puglisi, G., Ripepe, M., Rosi, M. (Eds.), The Stromboli Volcano: An Integrated Study of the 2002–2003 Eruption. Geophysical Monograph 182. American Geophysical Union, Washington, DC.

Ripepe, M., Delle Donne, D., Lacanna, G., Marchetti, E., Ulivieri, G., 2009. The onset of the 2007 Stromboli effusive eruption recorded by an integrated geophysical network. J. Volcanol. Geotherm. Res. 182 (3–4), 131–136. https://doi.org/10.1016/j.jvolgeores.2009.02.011.

Ripepe, M., Delle Donne, D., Genco, R., Maggio, G., Pistolesi, M., Marchetti, E., Lacanna, G., Ulivieri, G., Poggi, P., 2015. Volcano seismicity and ground deformation unveil the gravity-driven magma discharge dynamics of a volcanic eruption. Nat. Commun. 6. https://doi.org/10.1038/ncomms7998 art. no. 6998.

Ripepe, M., Lacanna, G., Pistolesi, M., Silengo, M.C., Aiuppa, A., Laiolo, M., Massimetti, F., Innocenti, L., Della Schiava, M., Bitetto, M., La Monica, F.P., Nishimura, T., Rosi, M., Mangione, D., Ricciardi, A., Genco, R., Coppola, D., Marchetti, E., Delle Donne, D., 2021. Ground deformation reveals the scale-invariant conduit dynamics driving explosive basaltic eruptions. Nat. Commun. 12 (1). https://doi.org/10.1038/s41467-021-21722-2 art. no. 1683.

Rosi, M., Pistolesi, M., Bertagnini, A., et al., 2013. Stromboli volcano, Aeolian Islands (Italy): present eruptive activity and hazards. Chapter 14. Geol. Soc. Lond. Mem. 37, 473–490. https://doi.org/10.1144/M37.14.

Sparks, R.S.J., 2003. Forecasting volcanic eruptions. Earth Planet. Sci. Lett. 210, 1–15. https://doi.org/10.1016/S0012-821X(03)00124-9.

Sparks, R.S.J., Cashman, K.V., 2017. Dynamic magma systems: Implications for forecasting volcanic activity. Elements 13, 35–40. https://doi.org/10.2113/gselements.13.1.35.

Sparks, R.S.J., Biggs, J., Neuberg, J.W., 2012. Monitoring volcanoes. Science 335, 1310–1311.

Stix, J., deMoor, M., Aiuppa, A., 2023. Sudden explosive eruptions: perspectives on plumbing systems, precursors, and warnings. In: Proc. IAVCEI 2023 Scientific Assembly, Rotorua, New Zeeland, p. 1007.

Swets, J.A., 1988. Measuring the accuracy of diagnostic systems, 240 (4857), 1285–1293. https://doi.org/10.1126/science.3287615.

Tamburello, G., Bitetto, M., Delle Donne, D., Aiuppa, A., 2023. Insights from CO_2/SO_2 Gas Molar Ratio Variations and Distribution at Stromboli Volcano, EGU General Assembly 2023, Vienna, Austria, 24–28 Apr 2023, EGU23–14757. https://doi.org/10.5194/egusphere-egu23-14757.

Valade, S., Lacanna, G., Coppola, D., Laiolo, M., Pistolesi, M., Delle Donne, D., Genco, R., Marchetti, E., Ulivieri, G., Allocca, C., Cigolini, C., Nishimura, T., Poggi, P., Ripepe, M., 2016. Tracking dynamics of magma migration in open-conduit systems. Bull. Volcanol. 78, 11. https://doi.org/10.1007/s00445-016-1072-x.

Vaselli, O., Tassi, F., Duarte, E., Fernandez, E., Poreda, R.J., Huertas, A.D., 2010. Evolution of fluid geochemistry at the Turrialba volcano (Costa Rica) from 1998 to 2008. Bull. Volcanol. 72, 397–410. https://doi.org/10.1007/s00445-009-0332-4.

Vergniolle, S., Métrich, N., 2022. An interpretative view of open-vent volcanoes. Bull. Volcanol. 84 (9), 1–45. https://doi.org/10.1007/s00445-022-01581-5.

Voloschina, M., Métrich, N., Bertagnini, A., Marianelli, P., Aiuppa, A., Ripepe, M., Pistolesi, M., 2023. Explosive eruptions at Stromboli volcano (Italy): a comprehensive geochemical view on magma sources and intensity range. Bull. Volcanol. 85 (6), 34. https://doi.org/10.1007/s00445-023-01647-y.

Williams-Jones, G., Stix, J., Heiligmann, M., Barquero, J., Fernandez, E., Gonzalez, E.D., 2001. A model of degassing and seismicity at Arenal Volcano, Costa Rica. J. Volcanol. Geotherm. Res. 108, 121–139. https://doi.org/10.1016/S0377-0273(00)00281-X.

Zuccarello, L., Burton, M.R., Saccorotti, G., Bean, C.J., Patanè, D., 2013. The coupling between very long period seismic events, volcanic tremor, and degassing rates at Mount Etna volcano. J. Geophys. Res. Solid Earth 118, 4910–4921. https://doi.org/10.1002/jgrb.50363.